Open access • Journal Article • DOI:10.1115/1.4042496

Application of Fractional Scaling Analysis for Development and Design of Integral Effects Test Facility — Source link

Milorad B. Dzodzo, Francesco Oriolo, Walter Ambrosini, Marco Enrico Ricotti ...+5 more authors

Institutions: Westinghouse Electric, University of Pisa, Polytechnic University of Milan, University of Zagreb ...+2 more institutions

Published on: 01 Oct 2019 - Journal of Nuclear Engineering and Radiation Science (American Society of Mechanical Engineers Digital Collection)

Milorad B. Dzodzo
Westinghouse Electric Company,
1000 Westinghouse Drive,
Cranberry Township, PA 16066
e-mail: dzodzomb@westinghouse.com

Francesco Oriolo
Department of Civil and Industrial Engineering,
Università di Pisa,
Via Diotisalvi 2,
Pisa I-56126, Italy

Walter Ambrosini
Department of Civil and Industrial Engineering,
Università di Pisa,
Via Diotisalvi 2,
Pisa I-56126, Italy

Marco Ricotti
Department of Energy,
Politecnico di Milano,
Via La Masa,
Milano 34-20156, Italy

Davor Grgic
FER,
University of Zagreb,
Unska 3,
Zagreb 10000, Croatia

Roberta Ferri
SIET S.p.A., UdP,
Via Nino Bixio 27/c,
Piacenza 29121, Italy

Andrea Achilli
SIET S.p.A., UdP,
Via Nino Bixio 27/c,
Piacenza 29121, Italy

Fosco Bianchi
ENEA,
UTFISSM,
Via Martiri di Monte Sole 4,
Bologna 40129, Italy

Paride Meloni
ENEA,
UTFISSM,
Via Martiri di Monte Sole 4,
Bologna 40129, Italy

Application of Fractional Scaling Analysis for Development and Design of Integral Effects Test Facility

The aim of this paper is to present a fractional scaling analysis (FSA) application for a system with interacting components where multiple figures of merits need to be respected during complex transient accident scenario with several consecutive time sequences. This paper presents FSA application to the International Reactor Innovative and Secure (IRIS) reactor and Simulatore Pressurizzato per Esperienze di Sicurezza 3 (SPES3) integral effects test (IET) facility. The FSA was applied for the small break loss of coolant accident (SBLOCA) on the direct vessel injection (DVI) line as the most challenging transient scenario. The FSA methodologies were applied for two figures of merits: (1) reactor and containment vessels pressure responses, and (2) reactor vessel water collapsed level response. The space decomposition was performed first. The reactor vessel and containment vessel were divided in components so that important phenomena and their consequences can be evaluated in each of them. After that, the time decomposition in consecutive time sequences was performed for the considered transient (DVI SBLOCA) based on the starts, or ends, of the defining events. The configuration of the system in each time sequence might be different and dependent on the control system actions connecting, or disconnecting, various components of the system due to the valves openings, or closings. This way, the important phenomena and their consequences can be evaluated for each component and time sequence. Also, this paper presents and discusses options for deriving nondimensional groups and calculation of distortions between prototype and model responses for complex transients containing multiple consecutive time sequences. The input data for scaling analysis are based on the results of RELAP/GOTHIC analysis performed for IRIS and RELAP analysis performed for SPES3. The scaling analysis was applied iteratively several times for different IRIS and SPES3 configurations. Based on the intermediate results, some components in the IRIS and SPES3 were redesigned so that the distortions between IRIS and SPES3 responses are decreased.
[DOI: 10.1115/1.4042496]

Introduction

The integral, modular, medium size pressurized water reactor (PWR) design of IRIS (International Reactor Innovative and Secure) is presented in Ref. [1]. The features of the integral reactor vessel design (see Fig. 1), which includes steam generators, pumps, and pressurizer inside the reactor vessel, together with the core and control rods, provide the safety-by-design approach by eliminating accidents, at the design stage, or decreasing their consequences and probabilities when complete accident elimination is not possible. The consequence of the integral design is that the IRIS integral vessel is larger than a traditional PWR pressure vessel, but the size of the IRIS spherical containment vessel (see Fig. 2) is a fraction of the size of corresponding loop reactors, resulting in a reduction in the overall size of the plant. The spherical, steel containment vessel allows designing a compact, higher design pressure, containment system. During the initial phases of a loss of coolant accident, the pressure in the IRIS containment is allowed to increase early in the accident, and thus the higher back pressure provides an inherent limitation to the inventory loss from the reactor coolant system. The IRIS design also includes a second means of core cooling via containment cooling. In the case that emergency heat removal system (EHRS) is not operational, direct

Manuscript received April 9, 2018; final manuscript received December 19, 2018; published online September 12, 2019. Editor: Igor Pioro.

cooling of the containment outer surface is provided and containment pressurization is limited to less than its design pressure. Thus, the safety-by-design approach allows a reduction and simplification of the passive safety systems.

The coupled RELAP and GOTHIC codes analysis of the reactor vessel and containment vessel interactions was performed to initially support IRIS design [2,3], and later on to support design optimization and provide an input for scaling analysis [4,5].

The Evaluation Model Development and Assessment Process (EMDAP), U.S. NRC Regulatory Guide 1.203 [6], was followed to evaluate adequacy of the applied codes (RELAP and GOTHIC) and provide areas for continued experimental data and analytical tool development. The first four EMDAP elements are presented in Fig. 3. Based on IRIS phenomena identification and ranking table (PIRT) [7], which is EMDAP element 1, step 4, two figures of merits are established. One is pressure response of the containment vessel, while the other is the water level in the reactor vessel. Also, based on the PIRT, it was concluded that continued experimental data and analytical tool development in the areas of steam generator; pressure suppression system, containment dry well (DW) and their interactions; emergency heat removal system; core, long-term gravity makeup system, automatic depressurization system (ADS), and pressurizer; and direct vessel injection system and reactor vessel cavity (CA) are important with respect to satisfying the safety analysis and licensing objectives of the IRIS program.

Besides multiple planned separate effect tests (SET), to address complex interactions between system components and to evaluate the IRIS response to transients and postulated accidents, an integral effects test (IET) facility, Simulatore Pressurizzato per Esperienze di Sicurezza 3 (SPES3), is designed as a part of EMDAP element 2—development of assessment base. The conceptual design and features of SPES3 IET facility are presented in Ref. [8]. The basic scaling criteria for designing SPES3 as a model for the IRIS prototype were:

- preserve volume ratio $V_{\text{model}}/V_{\text{prototype}} = 1/100$ for all components as much as possible;
- preserve the power to volume ratio;
- provide vessel wall thickness for the same fluid properties (prototypical pressure and temperature);
- preserve height of the vessels and internals;
- provide horizontal cross-sectional areas for fluid flow ratio in the 1/100, to maintain the same fluid velocities and residence times;
- preserve pressure drops;
- design vessels and internals shapes to preserve the ratio of water level and water volume.

The listed criteria lead to advantages and disadvantages. The advantages are that:

- The 1/100 volume ratio and the same power-to-volume ratio provide an adequate size of the test facility, which might be capable to decrease distortions due to the excessive accumulated heat of the side walls, connecting pipes, etc.;
- The use of the prototypical fluid allows avoiding distortions that would otherwise be caused by differences in fluid properties (i.e., the scaling analysis does not generate additional terms related to fluids property distortions). This would also make results interpretation easier;
- The full height provides prototypical distance between heat sources and heat sinks, which allows proper simulation of natural convection effects; both single-phase and two-phase natural convection loops can be simulated simultaneously;
- The properly scaled prototype and model fluid velocities and residence times in the loops are the same;
- Horizontal interphase areas (i.e., transfer area concentrations) are properly scaled;
- Liquid water levels are changing the same way as in the prototype vessels with the change of liquid volume, thus maintaining the same hydrostatic heads.

The disadvantages are that:

- As a consequence of preserving the same height, the vessels in the test facility are elongated (see Fig. 4) and the area of side vertical walls decreases only ten times (not 100 times as the volumes), which results in a ten times larger transfer area

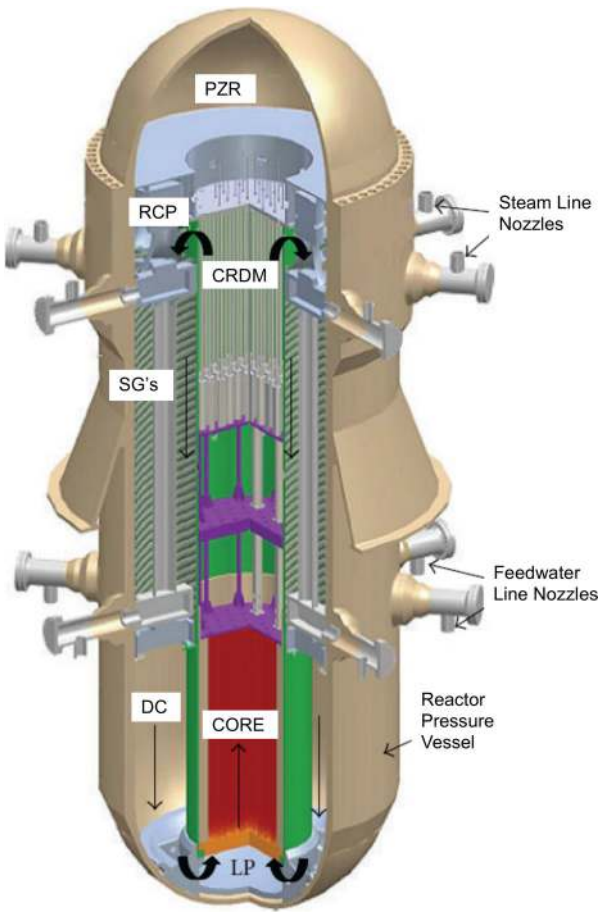

Fig. 1 International Reactor Innovative and Secure integral reactor vessel

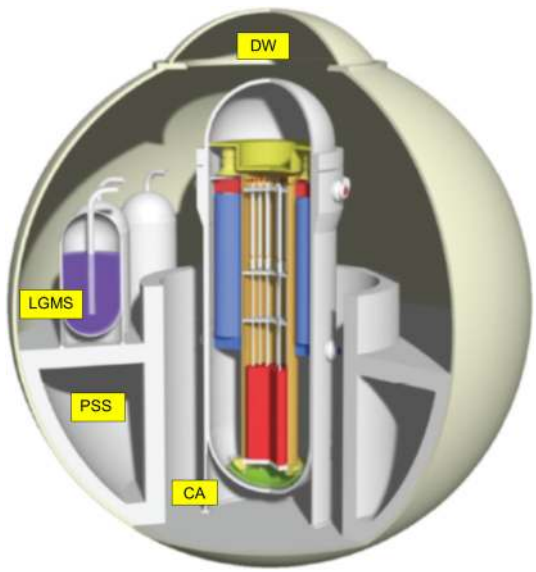

Fig. 2 International Reactor Innovative and Secure spherical containment vessel

concentrations for heat transfer (energy exchange) and wall friction (momentum exchange);
- Accumulated heat in side walls delays transient thermal responses;
- Some flow regimes and three-dimensional effects cannot be simulated due to the elongated vessels and narrow flow paths and additional SET might be needed for some components;
- Some components (e.g., heat exchangers and steam generators) might be represented with limited number of tubes (i.e., not ideal for reproducing side and heat exchanger bundle effects).

The RELAP analysis performed for SPES3 [9,10] was used to support design and later on to provide input data for scaling analysis (step 6 in element 2 of EMDAP) to evaluate the similarities, or differences, between prototype and model responses to various accidents transients scenarios.

There are opposing opinions if it is appropriate, or not, to utilize the same thermal hydraulic system code to provide an input for the scaling analysis used in EMDAP to support an assessment of the same code. An example of using thermal hydraulic code to support scaling of the test facility is presented in Ref. [11], where an intermediate ideally scaled virtual test facility was developed based on the model and used to support the real test facility design and specification of test initial and boundary conditions. More detailed discussion and support of implementing system evaluation models for scaling of experiments is available in Ref. [12]. This approach allows an iterative process of improvement of both: scaled test facility during design phase and applied system evaluation models.

The RELAP/GOTHIC performed analysis and fractional scaling analysis (FSA) methodology [13] were applied iteratively several times (see bold backward arrows in Fig. 3) for different IRIS and SPES3 configurations. Based on the intermediate results, some components in the IRIS and SPES3 facility were redesigned so that the expected distortions between IRIS and SPES3 responses are decreased. This iterative approach departs from the

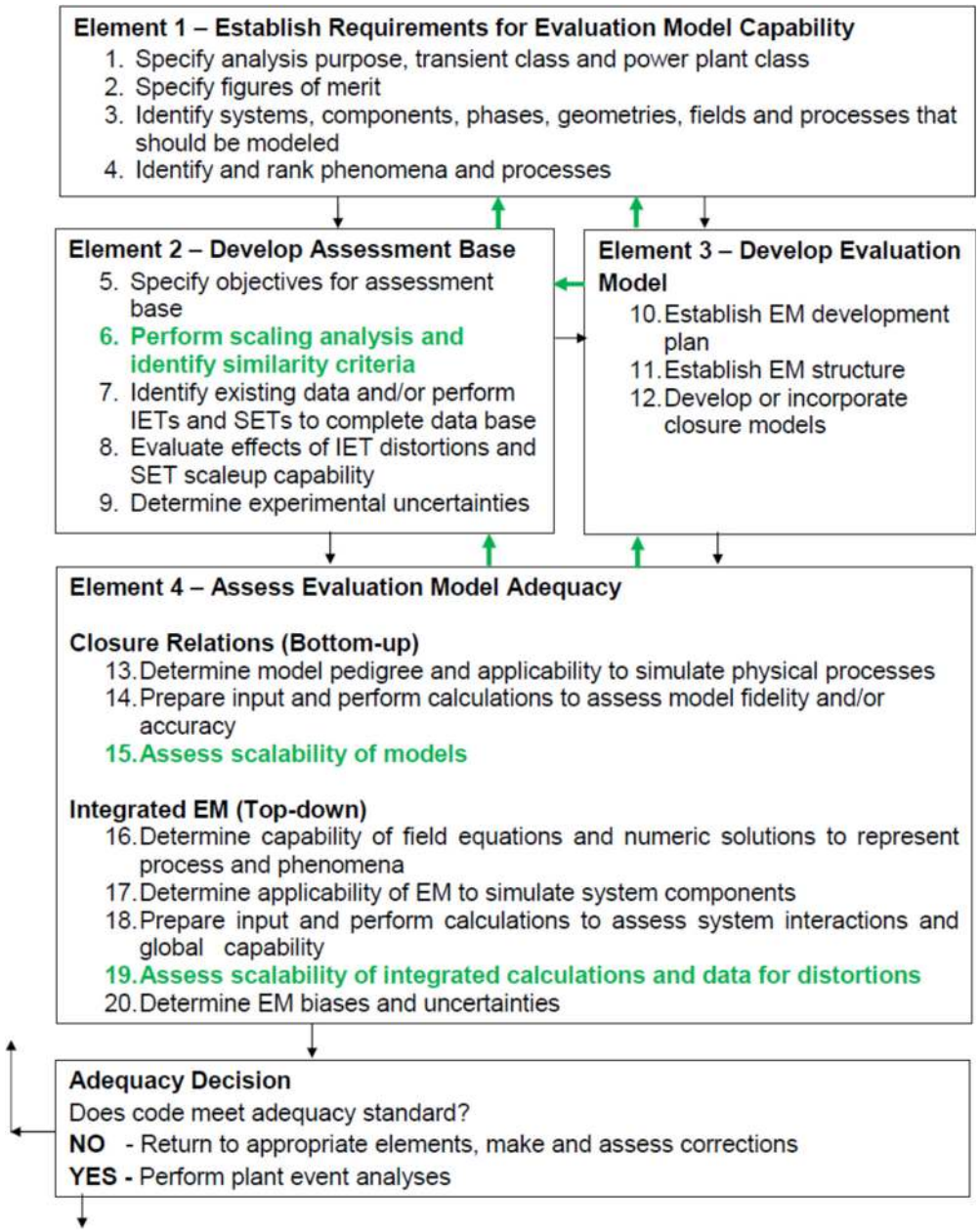

Fig. 3 The EMDAP flow chart

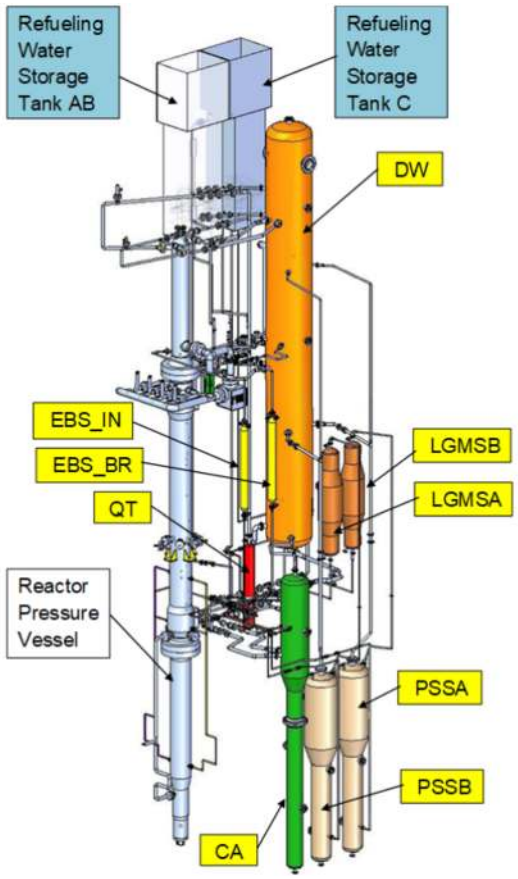

Fig. 4 Simulatore Pressurizzato per Esperienze di Sicurezza 3 general view

original EMDAP flow chart (where backward arrows are not present), but provides better design of IET facility so that expected distortions between prototypes and models might be decreased during IET design phase, before building it and starting tests (when any modification would delay test campaign and increase costs). Also, applied iterative approach provided an insight where additional development of IET facility instrumentation is needed, as number and distribution of measuring locations and frequency of measurement, as well as guidance to provide as flexible as possible IET facility design. An insight of performed design modifications is available in Ref. [10]. In some cases, the GOTIHC/RELAP models were improved as well by modifying or replacing heat transfer correlations for some heat exchangers, or by performing renodalization so that modeling of interactions between some components might be improved. The presented scaling analysis is related only to EMDAP element 2, step 6. Scalability of applied codes as specified in EMDAP element 4, steps 15 and 19 are not topics of this paper, although some gained information might be utilized to support this part as well.

This paper presents details of FSA methodology applied to the IRIS reactor and SPES3 IET. The FSA was applied for the small break loss of coolant accident (SBLOCA) on the direct vessel injection (DVI) line as the most challenging transient scenario. The FSA methodology and concepts were applied previously for various figures of merits as for vessel pressure response [14], vessel collapsed water-level response [15], and fuel peak cladding temperature response [16]. In this paper, the FSA methodologies were applied for two figures of merits: (1) containment vessel pressure response and (2) reactor vessel liquid water collapsed level response.

The space decompositions of the whole IRIS plant and SPES3 were performed first. The reactor vessel, containment vessel, and emergency heat removal system were divided in subcomponents and modules so that important phenomena and their consequences can be evaluated in each of them. After that, the time decomposition in consecutive time sequences was performed for the considered transient (DVI SBLOCA) based on the starts or ends of the events. This way, the important phenomena and their consequences can be evaluated for each time sequence.

Stage 1 SYSTEM DECOMPOSITION →	Stage 2 SCALE INDENTIFICATION →	Stage 3 TOP-DOWN SYSTEM SCALING ANALYSIS → ←	Stage 4 BOTTOM-UP PROCESS SCALING ANALYSIS
PROVIDE for each time sequence: System hierarchy IDENTIFY for each time sequence: Characteristic: Constituents Phases Geometries Processes	PROVIDE HIERARCHY FOR: Volumetric concentrations Area Concentrations Process time scales	PROVIDE: Conservation equations DERIVE: Scaling groups and characteristic time ratios ESTABLISH: Scaling hierarchy IDENTIFY: Important processes to be addressed in bottom-up process scaling analyses	PERFORM: Detailed scaling analysis for important processes DERIVE AND VALIDATE: Scaling groups

Fig. 5 Four stages of H2TS

The aim of this paper is to present FSA application and organization of the analysis for a complex system (which contains multiple interacting components) and transient accident scenario, which consists of multiple consecutive time sequences and where multiple figures of merits need to be respected at the same time. The configuration of the system in each time sequence might be different and dependent on the control system actions connecting, or disconnecting, various components of the system due to the valves openings, or closings. Also, this paper presents and discusses options of deriving nondimensional groups and calculation of distortions between prototype and model responses for complex transients containing multiple time sequences.

An Application of Fractional Scaling Analysis for Integral Effect Test Facility

For the scaling analysis, the EMDAP recommends the use of hierarchical, two-tiered scaling (H2TS) approach [17,18]. However, the new FSA approach [13,14,16,19], which evolved from H2TS, offers some advantages and might be applied as well.

Both methodologies, H2TS and FSA, use concepts from the hierarchical theory presented in Ref. [20] and the concept of time-scale modeling [21,22]. The same four stages (see Fig. 5) recommended for H2TS might be used for FSA. However, the FSA approach offers some advantages. One advantage is less complex hierarchy with only three levels (1—system, 2—components, and 3—processes), compared with eight levels in H2TS (1—system, 2—subsystems, 3—modules, 4—constituents, 5—phases, 6—geometrical configurations, 7—fields, and 8—processes). Another advantage is integral approach and simplified form of equations with each term representing effect of only one phenomenon. This simplifies the analysis and in some cases enables quantification of the PIRT table. This is important for the support of the top–down/system scaling analysis stage (stage 3 in Fig. 5) where the identification of the dominant phenomena to be addressed later on in the bottom–up/process scaling analysis stage (stage 4 in Fig. 5) needs to be performed. Thus, FSA is a quantitative methodology capable to scale time-dependent processes in a complex system of interacting components. This is especially important when a complex-postulated transient accident scenario consists of multiple consecutive time sequences. In that case, the system decomposition (stage 1 in Fig. 5) needs to be performed for each time sequence (see added text in green color in stage 1 column in Fig. 5) because the system configurations might be different during different time sequences. Also, integral approach of FSA analysis allows analysis to be easier performed directly at hierarchical level of choice if initial and boundary conditions and data needed at that level are available.

The complexity of both IRIS and SPES3 systems and capability to apply less complex hierarchy and an integral approach resulting in equations where each term represents effects of only one phenomenon are the main reasons why FSA is implemented for SPES3 IET.

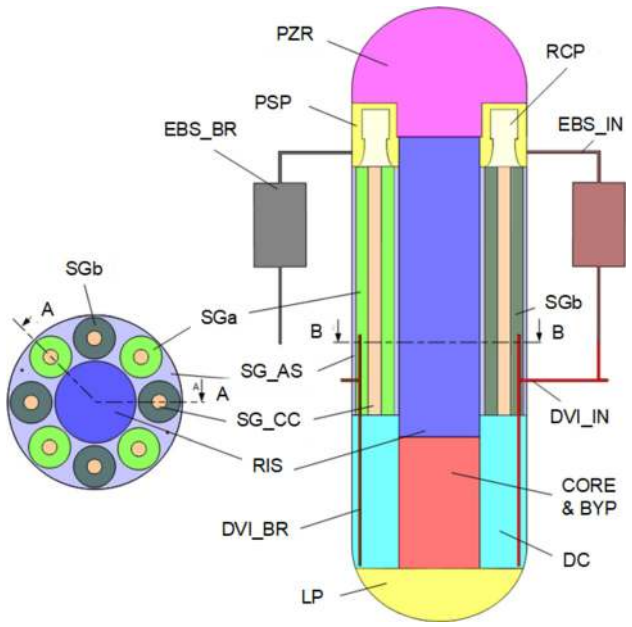

Fig. 6 International Reactor Innovative and Secure reactor pressure vessel space decomposition

System Space Decomposition

International Reactor Innovative and Secure Space Decomposition. The integral, modular, medium-size PWR design of IRIS is presented in Ref. [1]. The division of part of IRIS system needed for FSA analysis (reactor vessel and containment vessel) in components is created based on PIRT and the expected phenomena in each component, postulated break position, and distribution of the control valves capable to make connections and disconnections between components. This way, there is no need to introduce new components for different time sequences after system reconfigurations.

Due to the integral reactor vessel design, the steam generators, pumps, and pressurizer are together with the core inside the reactor vessel. The space decomposition of the reactor vessel in components is presented in Fig. 6. The reactor vessel components are also listed in Table 1 (components 1–16). The position of the postulated break and containment vessel components are presented in Fig. 7 and Table 1 (components 17–31). Also, the symbols (acronyms) used for each component are specified in Table 1. Components indicated by bold font in Table 1 are also present in the test facility.

It is worthwhile to note that only components taken into account in the FSA are specified in Table 1. The effects of the components, which are outside of the control volumes of interest, are taken into account as heat sources/sinks or break inflows/outflows in the interacting components inside the control volumes of interest.

For example, the EHRS components are neither specified in Table 1 nor used in FSA because the influence of the EHRS is taken into account as a heat source/sink for the steam generators. The heat source/sink fluxes are based on the results of the analyses performed on the entire IRIS/SPES3 Systems (including EHRS). The scaling analysis of the EHRS–SG connection SET is not part of this paper.

Simulatore Pressurizzato per Esperienze di Sicurezza 3 Space Decomposition. A description of SPES3 was presented in Ref. [8] and later on in Ref. [10]. The SPES3 decomposition (see Table 2) is performed so that it serves the purpose not only initially but also during the transient, so that all reconfigurations of the SPES3 System and closing/opening connections between its components may be taken into account.

Components present in IRIS and SPES3 are marked with symbols in bold in Tables 1 and 2. Note that the number of components for the SPES3 FSA is sometimes less than for IRIS when scaled IRIS components were subsumed in the SPES3 design. Components present in IRIS but not in SPES3 are marked by italic (not bold) symbols in Table 1. There are two reasons for this difference. First, the design of SPES3 is a simplified IRIS and some components are merged (i.e., not present in SPES3 as individual components). Examples are the merging of the steam generator annular space (SG_AS) and steam generator central column (SG_CC) with part of the riser (RIS). The second reason for the smaller number of components in SPES3 is that the model and analysis of this facility are performed with the RELAP code only, as opposed to the use of RELAP and GOTHIC codes for IRIS.

Table 1 International Reactor Innovative and Secure space decomposition

No	Symbol	Component description
1	**DC**	Down comer—annular region between reactor vessel and barrel
2	**LP**	Lower plenum—region below the bottom of active fuel
3	**CORE**	Core—cylindrical region with fuel inside the barrel
4	**BYP**	By-pass—cooling holes through reflector and annular space between reflector and barrel
5	**RIS**	Riser—region inside barrel between core and pressurizer
6	**PSP**	Pump suction plenum—annular part between SG modules and pressurizer
7	**RCP**	Reactor coolant pumps—eight internal pumps inside reactor vessel
8	**PZR**	Pressurizer—separated upper part of reactor vessel
9	***SGa***	Four steam generators connected to EHRSs 1 and 3 activated by reactor trip signal
10	***SGb***	Four steam generators connected to EHRSs 2 and 4 activated by LOCA mitigation signal
11	*SG_AS*	Steam generator annular space—region between barrel and reactor vessel and SG shrouds (*not present in SPES3*)
12	*SG_CC*	Steam generator central column—inner columns around which each SG helical bundle is wrapped (*not present in SPES3*)
13	**DVI_BR**	Direct vessel injection line in broken loop—DVI header and line up to break location
14	**DVI_IN**	Direct vessel injection line in intact loop—DVI header and line in intact loop up to LGMS squib valve
15	**EBS_BR**	Emergency Boration system in broken loop—EBS upper connection, tank, discharge line in the broken loop up to the EBS discharge valve
16	**EBS_IN**	Emergency Boration system in intact loop—EBS upper connection, tank, discharge line in the intact loop up to the EBS discharge valve
17	**DW**	Dry well—free space in containment except reactor vessel cavity
18	**CA**	Cavity—space in containment reactor vessel cavity
19	**PSS1**	Pressure suppression system tank 1—portion with water initially (PSSA in SPES3)
20	**VENT1**	Pipe connection of dry well and the PSS tank 1 (PSSB in SPES3)
21	*PSS2*	Pressure suppression system tank 2—portion with water initially
22	*VENT2*	Pipe connection of dry well and PSS tank 2
23	**LGMS1**	Long-term gravity makeup system tank 1
24	**LGMS2**	Long-term gravity makeup system tank 2
25	*PIPE1*	Pipe connection of PSS tank 1 and LGMS tank 1
26	*PIPE2*	Pipe connection of PSS tank 2 and LGMS tank 2
27	*PSS1B*	Pressure suppression system tank 1—steam and nitrogen initially
28	*PSS2B*	Pressure suppression system tank 2—steam and nitrogen initially
29	*VENT1B*	Upper pipe connection of dry well and the PSS tank 1
30	*VENT2B*	Upper pipe connection of dry well and the PSS tank 2
31	**QT**	Tank for ADS lines discharge (not presented in Fig. 7)

This eliminated the need for components necessary for the interaction between the two codes.

On the other hand, because SPES3 has three steam generators in this case, SPES3 has more steam generator components than IRIS (compare number of components with symbols in italic and bold in Tables 1 and 2). Instead of two for IRIS (see *SGa* and *SGb* in Table 1), three of them are present in SPES3 (see *SGA*, *SGB*, and *SGC*, in Table 2). This is because SPES3 steam generators were designed to address other possible IETs and SETs.

Time Decomposition of Postulated Transient Into Time Sequences. The details of time decomposition of the DVI SBLOCA transient in consecutive time sequences are presented in Ref. [23]. The low elevation DVI SBLOCA transient can be partitioned into time sequences characterized by the configuration and state of the system based on the start of the new events as:

- connections between the components (established by the valves openings and closings, or existence of pipe break);
- activity of some components like: pumps, core power, heat exchangers, and
- presence and distribution of some physical phenomena in components.

The time decomposition is needed because the ranking of all the processes taking place during the entire transient need to be achieved by comparing them first with the dominant process in each time sequence. After that, the importance (ranking) of the time sequences in relation to each other may be established. Thus, the important phenomena and their consequences can be evaluated for each time sequence.

The list of defining time events, start times, and short description of 22 time events for IRIS and SPES3 are specified in Table 3. The nature of time events is the same for both IRIS and SPES3, but the actual times at which each event occurs in the prototype and model are slightly different. It would be an ideal scenario that the test facility can reproduce the time events in the same consecutive order as the prototype. However, after comparing the start times for the SPES3 events, it can be noticed that some of the SPES3 events are not in the same consecutive order as IRIS time events. In Figs. 8–11, the location of each time event is presented and described (based on the IRIS modeling results). Due to the same nature of SPES3 time events (although shifted in time and some of them in different order then in IRIS), they are not presented. More detailed descriptions of time events and conditions defining their beginning are available in Ref. [23].

For each time sequence, the existing processes affecting the specified figures of merits are identified and taken into account for

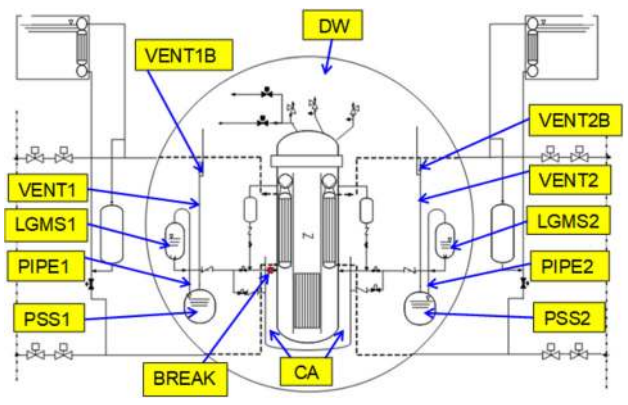

Fig. 7 International Reactor Innovative and Secure containment vessel space decomposition

Table 2 SPES3 space decomposition

No.	Symbol	Component description
1	**DC**	Down-comer—annular region between reactor vessel and barrel
2	**LP**	Lower plenum—volume at the bottom of the reactor vessel
3	**CORE**	Core—cylindrical region with fuel imitators inside barrel
4	**BYP**	By-pass—includes the imitator of cooling holes through reflector and annular space between reflector and barrel
5	**RIS**	Riser—cylindrical region inside barrel. It involves part of the volume which would correspond to SG_AS and SG_CC of scaled IRIS
6	**PSP**	Pump suction plenum—an irregularly shaped region located in the annular part of the reactor vessel above the SG modules
7	**RCP**	The reactor coolant pumps volume includes the external pump and corresponding piping
8	**PZR**	Pressurizer—upper part of the reactor vessel separated from the lower part of the vessel by an inverted hat shaped structure
9	***SGA***	This subvolume includes the primary side volume around the first steam generator closest to the riser with only one coil and 14 tubes in it
10	***SGB***	Primary side volume around the steam generator in the middle with only one coil and 14 tubes in it
11	***SGC***	Primary side volume around the outer steam generator with two coils and 14 tubes in each of them
12	**DVI_BR**	Direct vessel injection line in broken loop
13	**DVI_IN**	Direct vessel injection line in intact loop
14	**EBS_BR**	Emergency Boration system in broken loop
15	**EBS_IN**	Emergency Boration system in intact loop
16	**DW**	Dry well—all the free space in SPES3 containment except the reactor cavity
17	**CA**	Reactor cavity
18	**PSSA**	Pressure suppression system tank 1, lower portion (the portion which contains liquid water at the beginning of the transient) (PSS1 in IRIS)
19	**PSSB**	The lower portion of the pipe which connects the dry well and the PSS tank 1 (VENT1 in IRIS)
20	**LGMSA**	Long-term gravity makeup system tank 1
21	**LGMSB**	Long-term gravity makeup system tank 2
22	**QT**	Tank in which the ADS lines discharge

analysis. Based on the present processes, the agents of changes of the state variables, the fractional rates of changes, and the dimensionless groups as fractional changes (effect metrics) might be identified.

The Dimensionless Groups in Fractional Scaling Analysis. To quantify the effect of a changing state variable ψ by an amount $\delta\psi$, we can use the reference value ψ_0 and define fractional change (effect metric) as in Ref. [13]

$$\Omega = \frac{\delta\psi}{\psi_0} = \frac{\omega\,\psi\,\delta t}{\psi_0} = \frac{\Phi}{\psi_0}\delta t \tag{1}$$

where

$$\omega = \frac{\left(\frac{d\psi}{dt}\right)}{\psi} = \frac{\Phi}{\psi}\text{in}(1/\text{s}) \tag{2}$$

is the fractional rate of change of a state variable ψ, and

$$\Phi = \frac{d\psi}{dt} \tag{3}$$

is an agent of the change of a state variable ψ.

One advantage of this approach is that the governing equations related to figures of merits might be derived so that each term

Table 3 Time decomposition for DVI SBLOCA in IRIS and SPES3

IRIS event number	Event description for IRIS	IRIS time (s)	Event description for SPES3 (IRIS event number)	SPES3 time (s)
1	Break initiation	0	Break initiation (1)	0
2	SCRAM begins	31	SCRAM begins (2)	31
3	MFIV 1–4 closing	31	MFIV A, B, C closure starts (3)	31
4	MSIV 1–4 closing	31	MSIV A, B, C closure starts (4)	31
5	EHRS-AOV 1 and 3 opening	42	EHRS A and B opening starts (5)	32
6	RCP coastdown starts	147	RCP coastdown starts (6)	113
7	ADS stage I start opening (3 trains)	176	**Natural circulation begins through shroud valves (9)**[a]	133
8	EHRS-AOV 2 and 4 opening	178	EHRS C opening starts (8)	182
9	Natural circulation begins through shroud valves	188	**EBT A/B valve opening start (11)**	183
10	Flashing begins at core outlet	189	**ADS stage I start opening (3 trains) (7)**	184
11	EBS valves opening	195	**Flashing begins at core outlet (10)**	202
12	Natural circulation interrupted at SGs top	285	**EBT-RV connection uncovered (13)**	221
13	EBT-RV connection uncovered	395	**Natural circulation interrupted at SGs top (12)**	249
14	EBT broken loop empty	620	EBT-B empty (14)	481
15	LGMS tank of broken loop starts injection into cavity	1612	LGMS A/B valve opening start (15)	2150
16	LGMS intact loop starts to inject into RV through DVI intact loop	1730	**Containment and reactor vessel pressure equalization (17)**	2230
17	Containment and reactor vessel pressure equalization	1830	**LGMS A starts to inject into RV through DVI intact loop (16)**	2260
18	Steam and gas mixture flows again from RV to QT	3190	Steam and gas mixture flows again from RV to QT (18)	2270
19	ADS stage II starts opening	20,860	**Flow from RC to RV (loop A) starts (22)**	28,815
20	LGMS broken loop empty	20,873	LGMS B empty (20)	30,790
21	LGMS intact loop empty	22,300	**ADS stage II starts opening (19)**	31,569
22	Flow from RC to RV starts	49,116	**LGMS A empty (21)**	40,000

[a]Events in bold for SPES3 are not in the same consecutive order as events for IRIS.

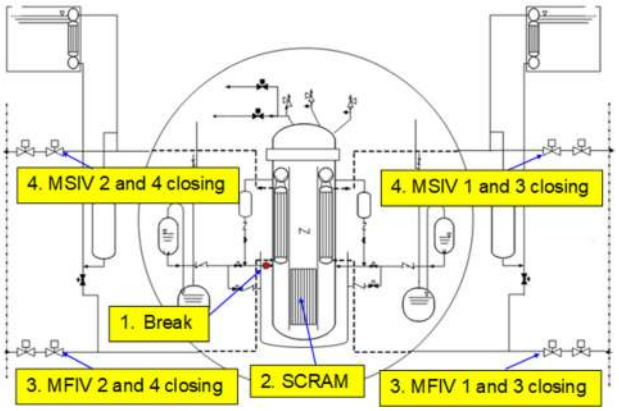

Fig. 8 Events defining time sequences: 1—break, 2—SCRAM, 3—MFIV closing, and 4—MSIV closing

represents influence of one process. The quantification and comparison of the terms provide an opportunity to quantify PIRT.

The list of considered processes and corresponding agents of changes and fractional rates of changes is presented in Tables 4 and 5 for reactor and containment vessels pressure responses, and reactor vessel collapsed water level, respectively.

Establishing Subvolume Ratios and Interactions Among Them. The stage 2 (scale identification) presented in Fig. 5 is for H2TS. This stage (scale identification) is different for FSA

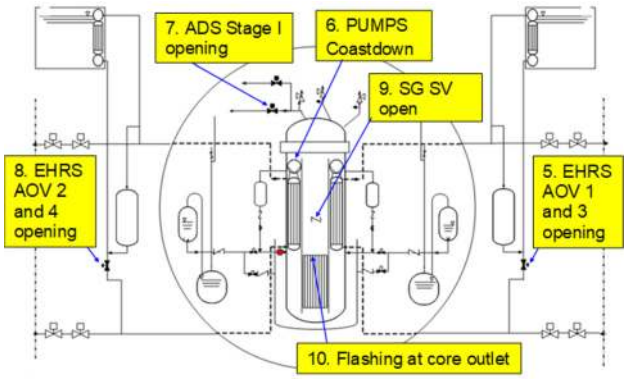

Fig. 9 Events defining time sequences: 5—ERHS AOV 1 and 3 opening, 6—pumps coastdown, 7—ADS stage I opening, 8—ERHS AOV 2 and 4 opening, 9—SG SV open, 10—flashing at core outlet

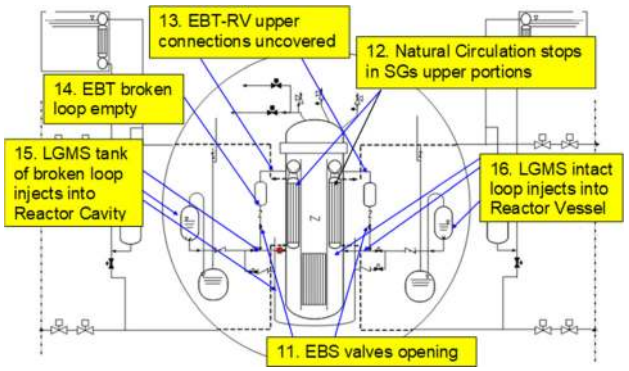

Fig. 10 Events defining time sequences: 11—EBS valves opening, 12—natural circulation stops in SG upper portions, 13—EBT-RV upper connections uncovered, 14—EBT broken loop empty, 15—LGMS tank of broken loop injects into reactor cavity, 16—LGMS intact loop injects into reactor vessel

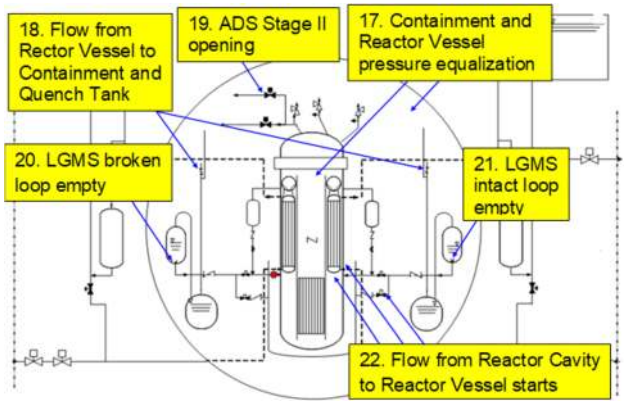

Fig. 11 Events defining time sequences: 17—containment and reactor vessels pressure equalization, 18—flow from reactor vessel to containment and quench tank, 19—ADS stage II opening, 20—LGMS broken loop empty, 21—LGMS intact loop empty, 22—flow from reactor cavity to reactor vessel starts

because of the smaller number of hierarchical levels and because of the integral approach to derive equations based on the summation of agents of changes effects. Instead of establishing volumetric and area concentrations and time scales for each hierarchical level, it is important to have information of the ratios of subvolumes occupied by single-phase liquid $V_{1\phi l}$, single-phase vapor $V_{1\phi v}$, saturated two-phase mixture $V_{2\phi}$, and noncondensable nitrogen gas V_{N_2}, inside the system volume (where $V = V_{1\phi l} + V_{1\phi v} + V_{2\phi} + V_{N_2}$) (see Fig. 12), so that compressibility of each subvolume might be properly taken into account. To capture this properly, the presented space decomposition (in stage 1) needs to be refined further for the applied GOTHIC/RELAP models by applying an adequate nodalization, as presented in Refs. [4,5], and [10].

Referring to Fig. 12, it must be pointed out that in the system control volume V:

- each subvolume, $V_{1\phi l}$, $V_{1\phi v}$, $V_{2\phi}$, V_{N_2}, may change in time, but the total volume V is constant;
- subvolumes may interchange mass (see for example mass flow rate terms $\dot{m}_{1\phi v,\mathrm{sat}\to 1\phi v}$ or $\dot{m}_{1\phi l\to 1\phi l,\mathrm{sat}}$) and energy (see interface terms $\dot{Q}_{\mathrm{int}}$) at the subvolumes boundaries;
- each subvolume might exchange heat with the surrounding walls (see terms $\dot{Q}_{\mathrm{wall}}$);
- the subvolumes may be placed anywhere in the control volume and need not necessarily be continuous;
- there might be mass flow rates terms (see $\dot{m}_{\mathrm{in}}$ or $\dot{m}_{\mathrm{out}}$) related to each field entering or exiting the control volume;

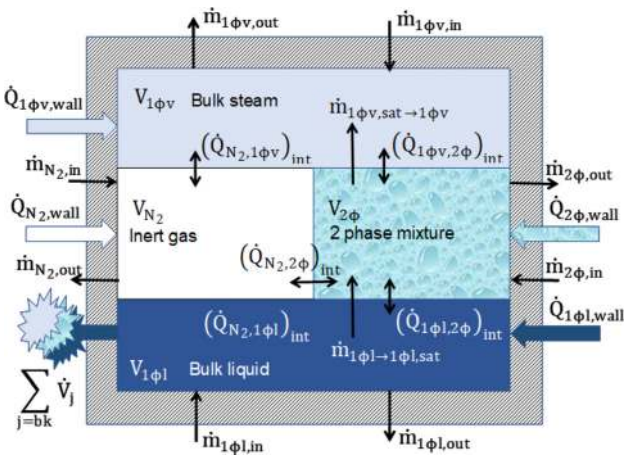

Fig. 12 Subvolumes V_j in control volume V

Table 4 Definitions of instantaneous fractional rates of changes for reactor vessel and containment vessel dimensionless pressure response equations

Description of agents of change—system or boundary effects	Instantaneous fractional rates of change $\omega_j(t)$
Break flow, inlet, and outlet $j=1$	$\omega_{\text{bk}} = \dfrac{\dot{V}_{\text{bk}}}{V\Delta p K_{s,\text{sys}}}$
Phase change by heating/cooling $j=2$	$\omega_{\dot{Q}_{2\phi}} = \dfrac{(v_{\text{fg}}/h_{\text{fg}})\dot{Q}_{2\phi}}{V\Delta p K_{s,\text{sys}}}$
Single phase thermal expansion/contraction by heating/cooling $j=3,4$	$\omega_{\dot{Q}_{1\phi}} = \dfrac{[\beta/(\rho\cdot c_p)]_{1\phi}\dot{Q}_{1\phi}}{V\Delta p K_{s,\text{sys}}}$
Expansion due to the heating by recirculation pumps $j=5$	$\omega_{\text{PP}} = \dfrac{[\beta/(\rho\cdot c_p)]_{l}\dot{P}_{\text{PP}}}{V\Delta p K_{s,\text{sys}}}$
Expansion/contraction of inert gas due to heating/cooling $j=6$	$\omega_{\dot{Q}_{\text{N}_2}} = \dfrac{\gamma-1}{\gamma}\dfrac{\dot{Q}_{\text{N}_2}}{V(\Delta p\cdot p)K_{s,\text{sys}}}$

Table 5 Definitions of instantaneous fractional rates of change for reactor vessel void fraction (water level) response

Description of agent of change—system or boundary effects	Instantaneous fractional rates of change $\omega_j(t)$
Break flow only vapor phase effect on α, $j=1$	$\frac{\dot{V}_{g,\text{in}}-\dot{V}_{g,\text{out}}}{V}$
Phase change by heating or cooling effect on α, $j=2$	$\frac{\dot{Q}_{2\phi}}{\rho_g h_{\text{fg}} V}$
Total break flow effect on $\dot{p}$, $j=3$	$\frac{\left(\sum_{j=\text{bk,ADS}}\dot{V}_j\right)\cdot\Psi_\alpha}{VK_{s,\text{sys}}}$
Phase change by heating or cooling effect on $\dot{p}$, $j=4$	$-\frac{(v_{\text{fg}}/h_{\text{fg}})\dot{Q}_{2\phi}\cdot\Psi_\alpha}{VK_{s,\text{sys}}}$
Single phase by thermal expansion or contraction by heating or cooling effect on $\dot{p}$, $j=1,v$, $j=5,6$	$-\frac{[\beta/(\rho\cdot c_p)]_j\left(\dot{Q}_{1\phi}\right)_j\cdot\Psi_\alpha}{VK_{s,\text{sys}}}$
Expansion due to heating by the recirculation pumps effect on $\dot{p}$, $j=7$	$-\frac{[\beta/(\rho\cdot c_p)]_l P_{\text{PP}}\cdot\Psi_\alpha}{VK_{s,\text{sys}}}$
Expansion of inert gas due to wall heating effect on $\dot{p}$, $j=8$	$-\frac{\gamma-1}{\gamma}\frac{\dot{Q}_{\text{N}_2}\cdot\Psi_\alpha}{V\cdot p\cdot K_{s,\text{sys}}}$

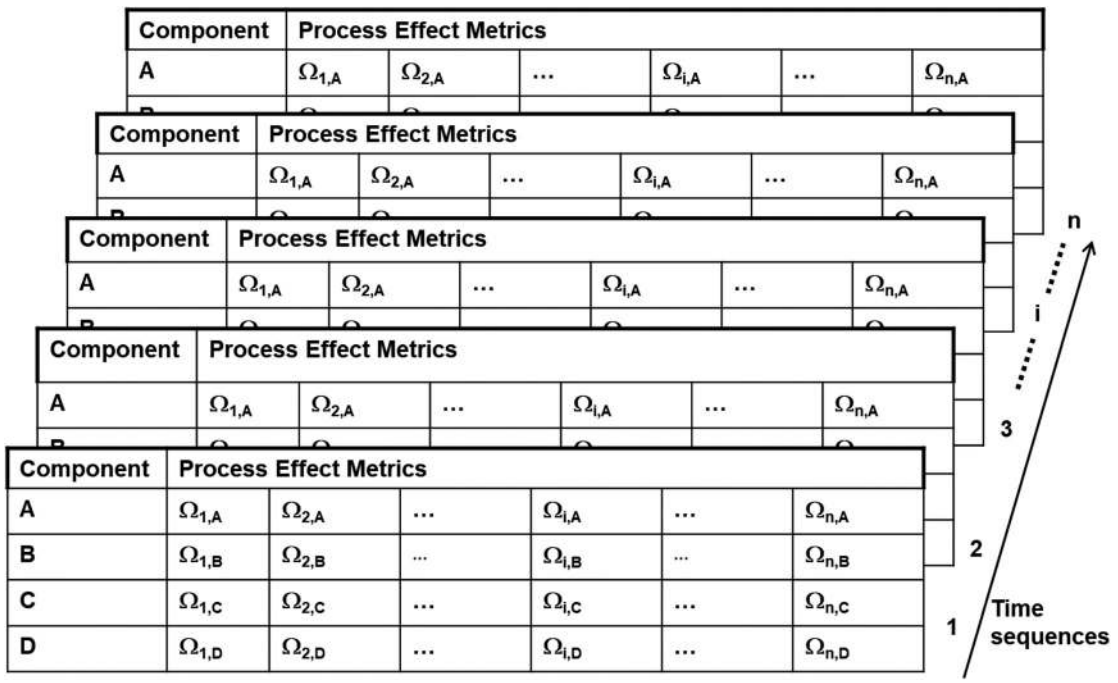

Fig. 13 System matrix for fractional scaling analysis for consecutive time sequences

- subcooled liquid, two-phase mixture, vapor, or noncondensable gas might be discharged from, or into the control volume (see term $\sum_{j=\text{bk,ADS}} \dot{V}_j$ for break flow and ADS volumetric flow rates).

All specified information need to be extracted from the applied GOTHIC and RELAP models and later on from the test facility so that comparisons between analysis and test results will be possible. Based on this, special attention was taken in planning an adequate two-phase flow measurement in piping between test facility components (tanks) [24–26], as well as collapsed water level inside the components (tanks).

The FSA analysis was performed for the reactor vessel and containment vessel pressure responses separately before the pressure equalization. The break flow was considered as boundary condition for both control volumes.

After pressure equalization, both control volumes were merged in one and FSA analysis was performed for the containment and reactor vessels as one control volume.

Top–Down System Scaling Analysis. The first step in stage 3, top–down system scaling analysis is to derive equations relevant to the specified figures of merits (see Fig. 5), followed by deriving dimensionless scaling groups (in FSA—the fractional changes, in fact the effect metrics—Ω). After that, the scaling hierarchy can be established by comparing quantified fractional changes (effect metrics) Ω for each process (agent of change), each system component, and each time sequence as presented in the system matrix for FSA in Fig. 13. It can be noted that for complex transients, the different effect metrics, Ω (in fact agent of changes, or processes), or groups of them might be dominant. This stage provides an analysis efficiency by identifying important processes to be addressed in stage 4, bottom–up process scaling analysis.

Reactor Vessel and Containment Vessel Pressure Response Equations. The assumptions and details of the derivation of the reactor vessel pressure response equation (4) based on FSA methodology, as well as Eqs. (5)–(12) explaining each term and normalization, are presented in Ref. [14]. Each term in Eq. (4) represents the influence of one phenomenon, in fact agent of change, affecting the pressure response

$$\dot{p} = \frac{1}{VK_{s,\text{sys}}}\left[\sum_{j=\text{bk,ADS}} \dot{V}_j + \frac{v_{\text{fg}}}{h_{\text{fg}}}\dot{Q}_{2\phi} + \sum_{j=1\phi l,1\phi v}\left(\frac{\beta_T}{\rho c_p}\dot{Q}\right)_j + \left(\frac{\beta_T}{\rho c_p}\right)_l P_{\text{pp}} + \frac{\gamma-1}{\gamma}\frac{\dot{Q}_{\text{N}_2}}{p}\right] \tag{4}$$

In Eq. (4), each term in the square bracket is a rate of volume change. For example:

- the sum of volumetric flow rates $\sum_{j=\text{bk,ADS}} \dot{V}_j$ leaving, or entering the control volume V through the break and valve openings;
- the rate of expansion or contraction due to the heating or cooling rate of phase change $\dot{Q}_{2\phi}$;
- the rates of volumes change due to thermal expansion or contraction by net heating or cooling rate, $\dot{Q}_{\text{net}}$ in single-phase regions (like for subcooled liquid $\dot{Q}_{1\phi,l}$, or vapor $\dot{Q}_{1\phi,v}$);
- the rate of volume change due to thermal expansion by adding pumping power P_{pp} in single-phase region of subcooled liquid l;
- the rate of volume changes due to the inert gas rate of heating or cooling $\dot{Q}_{\text{N}_2}$.

The denominator $VK_{s,\text{sys}}$ is the total system elasticity or "mechanical compliance," in which the system isentropic compressibility $K_{s,\text{sys}}$ is calculated as the volume fraction-weighted average of the isentropic compressibility's, $\kappa_s = c_v\kappa/c_p$ (where κ is isothermal compressibility), related to each subvolume V_j of the control volume V presented in Fig. 12

$$K_{s,\text{sys}} = \sum_{j=l,v,2\phi,\text{N}_2} K_{s,j} = \sum_{j=l,v,2\phi,\text{N}_2} \frac{V_j}{V}\cdot(\kappa_s)_j \tag{5}$$

The summation of isentropic compressibility's for each subvolume produces:

$$K_{s,\text{sys}} = \sum_{j=1\phi l,1\phi v}\left(\frac{c_v\kappa}{c_p}\right)_j \frac{V_j}{V} + \left\{\sum_{k=g,f}\alpha_k\left[\frac{v_{\text{fg}}}{h_{\text{fg}}}\left(\rho_k h'_k - 1\right) + \frac{\rho'_k}{\rho_k}\right]\right\}\frac{V_{2\phi}}{V} + \frac{1}{\gamma p}\frac{V_{\text{N}_2}}{V} \tag{6}$$

The terms with primes in the expression of the isentropic compressibility for two-phase mixture are, as in Ref. [27], enthalpy and density derivatives with respect to pressure along the saturation line

$$h'_k = \frac{1}{\rho_k} + T_{\text{sat}}\left[(c_p)_k\frac{v_{\text{fg}}}{h_{\text{fg}}} - \frac{\beta_k}{\rho_k}\right],\ k = g,f \tag{7}$$

$$\rho'_k = \left(\frac{\partial\rho_k}{\partial p}\right)_T\left[1 - T_{\text{sat}}\frac{v_{\text{fg}}}{h_{\text{fg}}}\left(\frac{\partial p}{\partial T}\right)_{\rho_k}\right],\ k = g,f \tag{8}$$

Equation (4) shows that a given amount of heat exchanged with any control subvolume might have different effects on the system pressure, depending on whether the control subvolumes contain single-phase or two-phase fluids. The system isentropic compressibility $K_{s,\text{sys}}$ and the denominator in the pressure response equation (4) are strongly influenced by the ratio of volumes filled with gas phase (steam and nitrogen), two-phase mixture, and liquid phase (liquid water). This might explain why at the beginning of small-break LOCAs (subsonic surge line flow), the initial ratio of vapor volume in the pressurizer and liquid water volume in the primary loop controls the initial primary system compliance and the initial depressurization rate. This can also explain why the results from various test facilities in Ref. [14] presented in FSA dimensionless form are all matching (following one pressure response curve). All test facilities were scaled for the same type of plants with the same initial ratio of volume in the pressurizer and liquid water volume in the primary loop. If this ratio is different, as in some new designs for small modular reactors, the response will be different.

The form of Eq. (4) might be used for containment vessel pressure response if adequate terms are taken into account, or excluded if not existing. For example, some terms listed in Table 4 are not necessary:

- Pump term ($j = 5$) is not present, since pumps are not part of the containment vessel;
- Before pressure equalization between reactor and containment vessels, only containment vessel volume is considered as a single control volume and inflow from the reactor vessel was taken into account via break terms ($j = 1$).
- After pressure equalization, reactor and containment vessels are coupled and considered as a single control volume: thus, the break terms ($j = 1$) cancel each other

In order to derive the pressure response equation for dimensionless pressure

$$p^* = \frac{p(t) - p_{\min}}{p_{\max} - p_{\min}} = \frac{p(t) - p_{\min}}{\Delta p},\ 0 \le p^* \le 1 \tag{9}$$

we might divide both sides of Eq. (4) by the reference pressure difference Δp (usually the initial difference between the primary system and the containment pressures).

Then, the pressure response equation for dimensionless pressure might be presented as summation of instantaneous fractional rates of changes (see Table 4), as functions of time, for various corresponding agents of changes

$$\frac{dp^*}{dt} = \sum_{j=\mathrm{bk},2\phi,l,v,\mathrm{PP},\mathrm{N}_2} [\omega(t)]_j = \sum_{j=1,6} [\omega(t)]_j \tag{10}$$

This is in agreement with already mentioned indication in [13,14] papers that only fractional rates of changes are needed for comparisons and calculation of distortions.

The instantaneous fractional change (effect metrics) Ω_j of dimensionless state variable might be obtained as a product of fractional rate of change of dimensionless state variable with an appropriate time interval (like time-step applied for calculation)

$$\Omega \approx \omega \cdot \delta t \tag{11}$$

The fractional rates of changes as functions of time in Eq. (10) (see Table 4) are evaluated for each time-step. This enables one to follow the time evolution of each of the fractional rates of changes during the entire transient and, therefore, to obtain a quantified PIRT over time without the need to make assumptions regarding the division of the transient into time sequences and extracting reference data for their initial conditions, since the relevance of each phenomenon might be compared with all others continuously during the entire time of transient.

This approach allows a continuous scaling analysis of complex transient accident scenarios and removes the need to normalize agents of changes and apply initial fractional rates of change at the beginning of each time sequence (as suggested in Table 1 [14]).

Guidance regarding the sequences progression for each time span may be obtained from the fractional rates of changes for each agent of change either from simulation, or test data (later on). The data at the beginning of each time sequence, or averaged data for the periods of times corresponding to the duration of time sequences, may be compared.

As mentioned earlier, in the section related to establishing subvolumes, adequate measurements in the test facility need to be specified and planned so that interactions between subvolumes can be measured, quantified, and compared with FSA obtained fractional rates of changes so that distortions between prototype and model responses might be calculated.

Also, certain data compatible with FSA need to be extracted from GOTHIC and RELAP models. To quantify terms in Eq. (10) and Table 4, additional calculations based on extracted data are needed for each time-step so that right volumes of subvolumes with different fluid properties and compressibility might be quantified.

The development and application of described FSA approach for IRIS and SPES3 reactor and containment vessels pressure responses based on GOTHIC and RELAP models input data are documented in Refs. [28–32]. Some results are presented in Refs. [23] and [33].

Reactor Vessel Void Fraction (Water Level) Response Equation. The reactor vessel liquid water collapsed level response scaling analysis was based on the entire reactor vessel void fraction response equations (12)–(14) derived by Wulff and Rohatgi [15]. The total reactor vessel volume V is considered as two-phase mixture volume $V_{2\phi}$, $V = V_{2\phi}$ in the first two terms of below equation:

$$\frac{d\alpha}{dt} = \frac{\dot{V}_{g,\mathrm{in}} - \dot{V}_{g,\mathrm{out}}}{V} + \dot{Q}_{2\phi}\left(\frac{1}{\rho_g h_{\mathrm{fg}} V}\right) - \dot{p}\Psi_\alpha \tag{12}$$

Each phase subvolume (see Fig. 12) is summed in order to obtain the total volume $V = \sum V_{1\phi l,j} + \sum V_{1\phi v,j} + \sum V_{2\phi,j} = \text{constant}$ and equal to the reactor vessel volume.

The time derivative of pressure in the last term is already available from Eqs. (4) and (12) might be rewritten as

$$\frac{d\alpha}{dt} = \frac{\dot{V}_{g,\mathrm{in}} - \dot{V}_{g,\mathrm{out}}}{V} + \dot{Q}_{2\phi}\left(\frac{1}{\rho_g h_{\mathrm{fg}} V}\right) - \frac{\Psi_\alpha}{VK_{s,\mathrm{sys}}} \left[-\sum_{j=\mathrm{bk},\mathrm{ADS}} \dot{V}_j + \frac{v_{\mathrm{fg}}}{h_{\mathrm{fg}}}\left(\dot{Q}_{2\phi}\right)_{\mathrm{net}} + \sum_{j=1\phi l,1\phi v}\left(\frac{\beta_T}{\rho c_p}\dot{Q}\right)_j + \left(\frac{\beta_T}{\rho c_p}\right)_l P_{\mathrm{pp}} + \frac{\gamma-1}{\gamma}\frac{\dot{Q}_{\mathrm{N}_2}}{p}\right] \tag{13}$$

The multiplier of the time derivative of pressure in the last term of Eqs. (12) and (13) is

$$\Psi_\alpha = \frac{\alpha\left(\rho'_g h_{\mathrm{fg}} + \rho_g h'_g\right) + (1-\alpha)\rho_l h'_l - 1}{\rho_g h_{\mathrm{fg}}} \tag{14}$$

The variables in Equation (14) are evaluated using mass-averaged pressures and temperatures for each phase in the whole volume and the void fraction α is the overall void fraction in the reactor vessel.

In order to obtain the fractional rates of changes and agents of changes for void fraction, equation (13) can be modified in a similar way as the pressure response equation. To note is that void fraction is already dimensionless $\alpha = \alpha^*$.

The reactor vessel void fraction response equation might be presented as summation of instantaneous fractional rates of changes (see Table 5), as functions of time, for various corresponding agents of changes

$$\frac{d\alpha^*}{dt} = \sum_{j=\dot{V}_g,\dot{Q}_{2\phi},\dot{V}_{\mathrm{bk},\hat{p}},\dot{Q}_{2\phi,\hat{p}},\dot{Q}_{l,\hat{p}},\dot{Q}_{v,\hat{p}},\mathrm{PP}_{\hat{p}},\dot{Q}_{\mathrm{N}_2,\hat{p}}} [\omega(t)]_j = \sum_{j=1,8} [\omega(t)]_j \tag{15}$$

The development and application of described FSA approach for IRIS and SPES3 reactor vessel collapsed water level responses are documented in Refs. [32] and [34]. Some results are presented in Refs. [10,23], and [35].

Evaluation of Distortions Between Prototype and Model Responses. The FSA provides quantification of the governing processes fractional changes (effect metrics) and an objective PIRT for a DVI-SBLOCA in IRIS and SPES3. In order to achieve these objectives and to calculate scaling distortions, the calculation of fractional rates of changes is needed.

The hierarchy of processes, established in the third stage of FSA, is performed through the calculation of fractional change (effect metric) Ω_j, since they quantify the agents of change effects (and order them by importance). The equality of fractional change Ω_j for model and prototype implies similarity of processes [13].

In order to calculate the normalized fractional change (effect metric) Ω_j^*, two approaches were proposed by [14]:

(1) each fractional rate of change is divided by the one of the break

$$\Omega_j^* = \frac{\omega_j}{|\omega_{\mathrm{bk}}|} \quad j = \mathrm{bk},\ 2\phi,\ 1\phi l,\ 1\phi v,\ \mathrm{N}_2 \tag{16}$$

(2) each fractional rate of change is divided by the absolute value of the fractional rates of changes summation (in fact, the absolute value of effective fractional rate of change, $\bar{\omega}$ symbol used in Ref. [14], or ω_e in Ref. [13].

$$\Omega_j^* = \frac{\omega_j}{\left|\sum_{j=\mathrm{bk},\,2\phi,\,1\phi l,\,1\phi v,\,\mathrm{N}_2} \omega_j\right|} = \frac{\omega_j}{|\bar{\omega}|} = \frac{\omega_j}{|\omega_e|} \tag{17}$$

At first sight, Eqs. (16) and (17) seem different. However, in Ref. [14], FSA was applied to large PWR vessel depressurization transients for which the fractional rate changes summation was almost equal to the dominant break term; hence, the results based on both equations were almost the same in their case.

In this work, the second approach is considered more suitable. Because of the small size of the break in the DVI line, the break jet is not powerful; thus, the other agents of change will compete with it, or may even be more important during some time sequences further away from the break initiation time sequence.

However, during some time sequences, numerical problems may occur if Eq. (17) is used. For example, during certain time periods, the sum of fractional rates of changes may become almost equal to zero and consequently the normalized fractional change (effect metric) may have high value. In order to avoid these problems, the normalized fractional changes (effect metrics) Ω_j^* are evaluated as follows:

$$\Omega_j^* = \frac{\omega_j}{\sum_{j=\mathrm{bk},\,2\phi,\,1\phi l,\,1\phi v,\,\mathrm{N_2}} |\omega_j|} \tag{18}$$

To decrease effects of GOTHIC and RELAP simulations and numerical oscillations, the eleven time steps-averaged fractional rates of changes ω_j are used in Eq. (18). Also, to exclude the initialization of calculation effects at the beginning of the time sequences, the fractional rates of changes ω_j of the first time-step are made equal to the second time-step values.

Then, using normalized fractional change (effect metric) for model (SPES3) and prototype (IRIS) as dimensionless groups, the scale distortions for containment vessel pressure responses are calculated as their ratios, as suggested in Ref. [15]

$$D_j = \Omega_{j,M}^*/\Omega_{j,P}^* \quad j = \mathrm{bk},\ 2\phi,\ 1\phi l,\ 1\phi v,\ \mathrm{N_2} \tag{19}$$

The scale distortions for reactor vessel collapsed water-level response are calculated the same way

$$D_j = \Omega_{j,M}^*/\Omega_{j,P}^* j = \dot{V}_g, \dot{Q}_{2\phi}, \dot{V}_{\mathrm{bk},\dot{p}}, \dot{Q}_{2\phi,\dot{p}}, \dot{Q}_{l,\dot{p}}, \dot{Q}_{v,\dot{p}}, PP_{\dot{p}}, \dot{Q}_{\mathrm{N_2},\dot{p}} \tag{20}$$

The criteria adopted to evaluate scale distortions, i.e., to assess if the test facility (model) and the plant (prototype) are well scaled or not, were presented in the same Ref. [15], where three regions are identified:

(1) if $1/2 < D_j < 2$ the phenomenon is acceptably scaled (the difference is less than 100%);
(2) if $1/3 < D_j < 1/2$ or $2 < D_j < 3$ the phenomenon presents a distortion of the first grade;
(3) if $D_j < 1/3$ or $D_j > 3$ the phenomenon presents a distortion of the second grade. (21)

It is also important to evaluate if the present distortion is conservative or nonconservative. For example, the scale distortion in a model would be considered to be a conservative if the corresponding process (agent of change) in the model (test facility) increases containment pressure, or reduces coolant inventory in the reactor vessel, etc.

In the case when $D_j < 0$, the fractional change (effect metrics) Ω_j has different sign in the prototype and in the model, and the phenomenon is completely distorted. This might occur during one time sequence (or part of it) if solid structure in the prototype acts as a heat source and causes boiling of the surrounding liquid; while in the model, the corresponding solid structure acts as a heat sink and causes condensation of the surrounding steam. The number of time sequences (or duration of time periods inside them) with similar situations need to be either eliminated or minimized by proper scaling and design of the model.

However, the specified criteria might need to be re-evaluated because of the different ways that normalized fractional changes (effect metrics) Ω_j^* were calculated here and in Ref. [15]. Instantaneous $(\omega_j)_t$ instead normalized at the beginning of time sequences $(\omega_j)_0$ fractional rates of changes are used in Eq. (18). Also, Eq. (18) might produce smaller values for normalized fractional changes (effect metrics) Ω_j^* than Eq. (17) due to the difference in the denominator calculation. The decreasing peaks of calculated normalized fractional changes (effect metrics) Ω_j^*, might also affect the calculated distortions.

In some cases, it is important to match the prototype and model normalized fractional changes (effect metric) for the dominant phenomena first (if possible). Then, the distortions for less important phenomena might be tolerated. On the other side, there might be some time sequences when all phenomena might have almost the same impact and consequently all distortions need to be small. So, the matrix of fractional changes (effect metrics) needs to be evaluated first for all time sequences and existing phenomena in each of them (see Fig. 13).

Thus, the importance of each time sequence needs to be evaluated based on their duration, present phenomena, and their

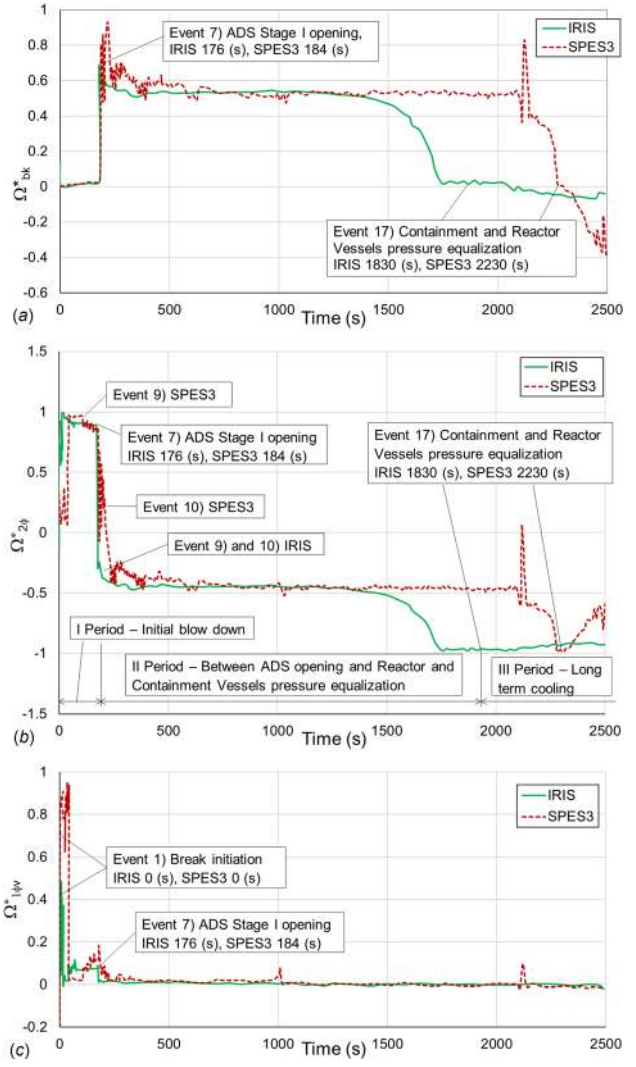

Fig. 14 Normalized fractional changes (effect metrics) for pressure response as a function of time of: (*a*) break Ω_{bk}^*, (*b*) two phase heat transfer $\Omega_{2\phi}^*$, and (*c*) single-phase heat transfer to vapor $\Omega_{1\phi v}^*$

dominance (or nondominance), and effects on the control systems decisions to keep the time sequences in the model in the same consecutive order as in the prototype. Based on all this, the criteria might be developed to determine how well-scaled and designed model needs to be during each time sequence. So, the criteria for the distortion acceptability might not be the same for different time sequences. Finally, if the same consecutive order of time sequences as in the prototype cannot be achieved in the model, the scaling analysts, test facility designer, and test program planners need to decide, based on the mentioned criteria, if the test can be performed as continuous, or it might need to be divided in several segments of several consecutive time sequences by providing adequate initial and boundary conditions for each segment separately.

However, evaluation of distortions based on the instant values (at the beginning of time sequences) might produce wrong conclusions if processes are oscillatory, or if the process does not exist in the prototype (when $\Omega_{j,P} \approx 0$) at that moment.

To avoid this, the prototype and model fractional changes (effect metrics) histories might be compared over time. Ideally, the time histories would be overlapping, but because of the delays of some processes and different order and duration of the prototype and model time sequences, usually they do not. From the time histories, the periods of oscillatory behavior of some processes, nonexistent processes (or very weak, or sporadically present) in the prototype (when $\Omega_{j,P} \approx 0$), opposite behaviors of the model and prototype processes ($\Omega_{j,P} > 0$ and $\Omega_{j,M} < 0$, or vice versa), and differences in fractional change (effect metrics) trends ($\Omega_{j,P}$ increases and $\Omega_{j,M}$ decreases, or vice versa) and magnitudes ($|\Omega^*_{j,P}| \gg |\Omega^*_{j,M}|$, or vice versa) in the prototype and model might be noticed and the existing time sequences might be divided into additional subsequences, or the new time sequences introduced.

Combination of these approaches might provide better understanding of why prototype and model have different responses and unacceptable distortions. It also provides an opportunity to capture situations when combinations of different processes in the prototype and model produce qualitatively similar responses for monitored figures of merits (risking claim that the model is well scaled, but due to the wrong reasons).

Establishing Scaling Hierarchy and Identification of Important Processes. Based on the quantified fractional rates of changes, it could be concluded that processes related to the compressibility of water in liquid phase and noncondensable gases can be neglected for all time sequences because their fractional rates of changes values ($\omega_{1\phi l}$ and ω_{N_2}) are several orders of magnitude smaller than for other processes. Other processes (ω_{bk}, $\omega_{2\phi}$, and $\omega_{1\phi v}$) need to be evaluated and compared with each other for each time sequence separately. In Fig. 14, the comparison of prototype and model normalized fractional changes for containment vessel pressure response for break Ω^*_{bk}, two-phase heat exchange $\Omega^*_{2\phi}$, and single-phase heat exchange with steam (vapor) $\Omega^*_{1\phi v}$ are presented for the first 2500 s, which includes the first 17 time events (including the reactor vessel and containment vessel pressure equalization).

It could be noticed that for the break normalized fractional change Ω^*_{bk} (see Fig. 14(*a*)), the most important event and process is the start of ADS stage I opening (event 7). The ADS stage I steam supply continues to dominate close to the containment and reactor vessel pressure equalization (event 17). The initial break in DVI line (event 1) is not so important because the volumetric flow rate of the liquid phase is not high. However, it could be noticed that during that period (between events 1 and 7), the normalized fractional change of two-phase heat exchange $\Omega^*_{2\phi}$ (see Fig. 14(*b*)) is dominant and related to DVI line break high pressure and temperature liquid water flashing in the containment lower pressure atmosphere. The normalized fractional change of single-phase heat exchange with steam (vapor) $\Omega^*_{1\phi v}$ (see Fig. 14(*c*)) is noticeable only during the first seven time sequences. After that, this process can be neglected.

Practically, the period before containment and reactor vessel pressure equalizations can be divided in two (see Fig. 14(*b*)). The first one, initial blow down before ADS stage I opening (event 7), when $\Omega^*_{2\phi} \approx 1$ is dominant and $\Omega^*_{1\phi v}$ present, and the second one (between events 7 and 17) when water in reactor vessel starts to flash and later on boils, while condensation of the steam in the containment vessel $\Omega^*_{2\phi} \approx -0.5$ is balancing the steam release from the ADS stage I $\Omega^*_{bk} \approx 0.5$. The model longer release of steam from ADS stage I and the delay of the containment and

Table 6 Distortions for containment vessel pressure response at the beginning of time events

Time event	Times t_M/t_P (s)	$D_{br} = \frac{\Omega^*_{br,M}}{\Omega^*_{br,P}}$	$D_{2\phi} = \frac{\Omega^*_{2\phi,M}}{\Omega^*_{2\phi,P}}$	$D_{1\phi,v} = \frac{\Omega^*_{1\phi,M}}{\Omega^*_{1\phi,P}}$	Dominant phenomena
Based on the containment vessel as control volume and instant data					
2, 3, 4	*31/31*	***0.43*** = 0.0036/0.0059	*0.14* = 0.136/**0.959**	*26.2* = **0.860**/0.033	2ϕ in both; *P* and *M*. Flashing of the liquid break.
5	*32/42*	***0.29*** = 0.002/*0.069*	*0.15* = 0.150/**0.973**	*46.9* = **0.847**/0.018	
6	*113/147*	**0.67** = 0.013/0.020	**1.03** = **0.924/0.901**	**0.82** = 0.061/0.074	
7	***184***/*176*	*17.9* = **0.581**/0.032	*0.27*=0.237/**0.868**	**1.97** = 0.181/0.092	
8	*182/178*	**0.77** = 0.025/0.035	**1.00** = **0.867/0.863**	**1.11** = 0.105/0.095	
9	***133***/*188*	*0.02* = 0.015/**0.697**	*−3.15*= **0.885**/−0.281	*4.60* = 0.098/0.021	
10	***202***/*189*	**0.79** = **0.548/0.690**	*−1.34* = 0.382/−0.285	***2.94*** = 0.068/0.023	br *(in fact ADS stage I)*, in both *P* and *M* after flashing and two phase heat transfer in the core starts.
11	***183***/*195*	**1.20** = **0.796/0.662**	*0.07* = −0.024/−0.326	*16.3* = 0.178/0.011	
12	***249***/*285*	**1.03** = **0.572/0.554**	**0.95** = −0.415/−0.437	**1.51**= 0.012/0.008	
13	***221***/*395*	**1.72** = **0.925/0.537**	*0.05* = −0.023/−0.455	*7.39* = 0.050/0.007	
14	*481/620*	**1.08** = **0.584/0.538**	**0.87** = −0.396/−0.453	***2.35*** = 0.019/0.008	
15	*2150/1612*	**1.07** = 0.391/0.365	**0.96** = **−0.634/−0.608**	**1.03** = 0.00074/0.00072	2ϕ , condensation in both;*P* and *M* containments.
16	***2260***/*1730*	*10.6* = 0.214/0.020	**0.80** = **−0.785/−0.977**	*−0.52* = −0.00081/0.00157	
Based on the containment and reactor vessels as control volume and 11 time steps averaged data					
17	***2230***/*1830*		**0.916** = −0.469/**−0.512**	**1.11** = **−0.526**/−0.475	2ϕ 50%, condensation and 1ϕ,*v* 50%, steam cooling in both *P* and *M*.
18	*2270/3190*		**0.589** = −0.436/**−0.739**	***2.40*** = **−0.559**/−0.233	
19	***31,569***/*20,860*		*−139* = −0.209/0.0015	**0.824** = **−0.789/−0.957**	1ϕ,*v* steam cooling in both *P* and *M*.
20	*30,790/20,873*		−282 = −0.275/0.000 97	**0.892** = **−0.718/−0.959**	
21	***40,000***/*22,300*		*−11.5* = −0.138/0.012	*−0.932* = **−0.855/0.917**	1ϕ,*v* steam cooling in *M*, steam heating in *P*.
22	***28,815***/*49,116*		**0.595** = −0.282/−0.474	*−1.400* = **−0.701/0.500**	

Note: **well scaled**, ***distortion first class***, *distortion second class*, *opposite behavior*.

rector vessels pressure equalization can be explained by the well-known distortion of the full height test facility caused by excessive heat transfer area of the reactor and containment vessels vertical walls and heat accumulated in them.

After containment and reactor vessel pressure equalization, the third period of long-term cooling starts. The control volume contains the reactor vessel as well and condensation of steam in the containment and in the reactor vessel (in fact steam generator, acting as a condenser) is the dominant process ($\Omega^*_{2\phi} \approx -1$).

It could be concluded that during the first and second periods of transient (before containment and reactor vessels pressure equalization), the model response is qualitatively in agreement with the prototype response (from the standpoint of the present and dominant processes), but with some delay in time.

Table 6 presents distortion values for this period based on the fractional changes values at the beginning of time events. The values of fractional change (effect metric) for model Ω_M and prototype Ω_P used to calculate distortions are presented as well. The dominant fractional changes (effect metric) are in bold. The opposite behavior ($D_{2\phi} < 0$) for $\Omega^*_{2\phi}$ can be noticed for events 9 and 10. The main reason for the opposite prototype and model behavior is the earlier occurrence of 9 and slight delay of 10 in the model response (see Fig. 14(*b*)). However, it might be concluded that the time histories of the normalized fractional changes for prototype and model agree qualitatively between 0 and 500 s and the model follows (with the small delay) the prototype response.

After containment and reactor vessels' pressure equalization, the prototype and model normalized fractional change of two-phase heat exchange $\Omega^*_{2\phi}$, and the normalized fractional change of single-phase heat exchange with steam (vapor) $\Omega^*_{1\phi v}$ contribute almost equally $\Omega^*_{2\phi} \approx \Omega^*_{1\phi v} \approx -0.5$ up to 3500 s. From 3500 to 20,000 s, the prototype and model normalized fractional changes of single-phase heat exchange with steam (vapor) are dominant $\Omega^*_{1\phi v} \approx -1$ (with short periods of $\Omega^*_{1\phi v} \approx 1$ for model) and $\Omega^*_{2\phi} \approx 0$.

Figure 15 compares the prototype and model normalized fractional changes for two-phase heat exchange $\Omega^*_{2\phi}$, and single-phase heat exchange with steam (vapor) $\Omega^*_{1\phi v}$ for the period between 20,000 and 55,000 s. This period is relevant for events 19 to 22. It could be noticed that the model time events 19, 20, and 21 are delayed, while the time event 22 occurs earlier.

Between 20,000 and 25,000 s, the normalized fractional change for two-phase heat exchange for the prototype is $\Omega^*_{2\phi,P} \approx 0$, while for the model, it is $\Omega^*_{2\phi,M} \approx -0.4$ and oscillates between -0.6 and -0.2 (see Fig. 15(*a*)). Events 19–21 for the prototype occur during this period, while for the model, they occur between 30,000 and 40,000 s when the model $\Omega^*_{2\phi} \approx -0.2$. This explains high $D_{2\phi}$ distortions for events 19–21 in Table 6.

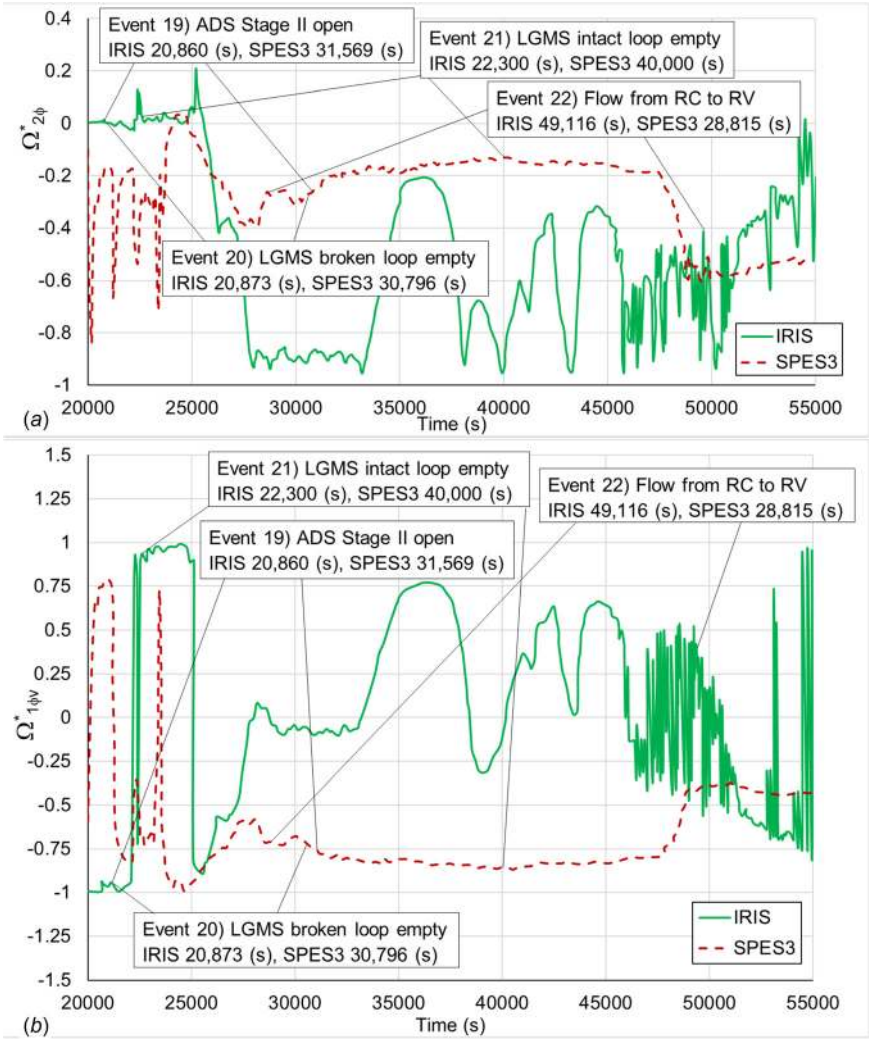

Fig. 15 Normalized fractional changes (effect metrics) for pressure response as a function of time of: (*a*) two phase heat transfer $\Omega^*_{2\phi}$, (*b*) of single-phase heat transfer to vapor $\Omega^*_{1\phi v}$

In Fig. 15(*b*), the comparison of prototype and model of single-phase heat exchange to vapor normalized fractional changes $\Omega^*_{1\phi v}$ is presented. It can be noticed that between 20,000 and 25,000 s, $\Omega^*_{1\phi v,P}$ is dominant for the prototype, but switches from −1 to 1 after ADS stage II opening at 20,860 s and drops to −0.8 after 25,000 s. After that, it gradually increases and reaches −0.1 around 28,000 s and stays there up to 33,000 s and then starts to oscillate between 0.7 and −0.7. The oscillatory behavior of $\Omega^*_{1\phi v,M}$ for the model is present between 20,000 and 25,000 s and after that it is most of the time $\Omega^*_{1\phi v,M} \approx -0.8$ (starting from −1 and ending at −0.45). The calculated distortions presented in Table 7 are affected by the delays of events in the model and different values of prototype and model fractional changes.

Unfortunately, the decrease of distortions for this period of transient by redesigning the test facility is more difficult because there is no presence of the dominant processes. Instead, two not so intensive processes are competing with each other. The main difference is that in the model, both are almost all the time present with $\Omega^*_{2\phi,M} \approx -0.2$ and $\Omega^*_{2\phi,M} \approx -0.8$, while in the prototype, $\Omega^*_{2\phi,P}$ and $\Omega^*_{1\phi v,P}$ are switching their presence. However, it is interesting to note that in spite of prototype and model different responses for individual processes, the combination of processes produces qualitatively similar responses for monitored figure of merits (see Figs. 18 and 19).

The comparison of prototype and model normalized fractional changes for void fraction of the reactor vessel for vapor volumetric flow rate $\Omega^*_{\dot{V}_g}$ and two-phase change heating/cooling $\Omega^*_{\dot{Q}_{2\phi}}$ are presented for the entire transient in Figs. 16 and 17 (see the lower figures from 0 to 100,000 s), respectively. The responses at the beginning of transients are presented in the upper figures (from 0 to 5000 s in Fig. 16, and from 0 to 500 s and from 0 to 5000 s, for Fig. 17). Other normalized fractional changes Ω^*_j ($j = 3$–8 in Eq. (20)) related to the containment vessel pressure response are not significant. Thus, Table 7 presents only distortions $D_{\dot{V}_g}$ and $D_{\dot{Q}_{2\phi}}$ for the significant normalized fractional changes. An insight into the normalized fractional rate of change time histories in Figs. 16 and 17 might help to understand and evaluate distortions presented in Table 7.

The normalized fractional changes for vapor volumetric flow rate $\Omega^*_{\dot{V}_g}$ time histories for the prototype and model (see Fig. 16) are in qualitative agreement (with some exceptions in short periods) up to 20,000 s. After that (see lower Fig. 16), the prototype $\Omega^*_{\dot{V}_{g,P}} \approx -0.4$ indicates continuous outflow of the mixture of vapor and noncondensable gases from the reactor vessel to the containment vessel. During the same period, the model $\Omega^*_{\dot{V}_{g,M}} \approx 0$ is close to zero, but almost all the time negative ($\Omega^*_{\dot{V}_{g,M}} < 0$).

The most challenging distortion evaluation is for two-phase change heating/cooling normalized fractional changes $\Omega^*_{\dot{Q}_{2\phi}}$ because of the processes oscillatory behavior (see Fig. 17). In Fig. 17, the initial blow-down period before ADS stage I opening (I period) and the beginning of the second period are presented (up to 500 s). It can be concluded that the two-phase change (flashing and condensation) is dominant and $\Omega^*_{\dot{Q}_{2\phi}}$ oscillates between −0.95 and 0.95 during the first period. The upper Fig. 16 indicates that during the first period, $\Omega^*_{\dot{V}_g}$ is small. This is because before the ADS stage I opening, the liquid phase flows through the DVI line break. It can be concluded that the dominant phenomenon is well scaled.

Based on the upper Figs. 16 and 17 for the first 5000 s, it can be concluded that during the second period (after ADS stage I opening and before containment and reactor vessels pressure equalization), the vapor volumetric flow outlet $\Omega^*_{\dot{V}_g} \sim -0.5$ is compensated by water flashing and later on boiling steam generation, $\Omega^*_{\dot{Q}_{2\phi}} \sim 0.5$. Thus, both phenomena are equally important. Based on the heat fluxes and volumetric flow rates, this is the most intensive portion of the transient. Table 7 indicates that only volumetric flow rates are well scaled at some time events. Two-phase change heating and cooling is not formally well scaled based on the values at the event starting times due to the

Table 7 Distortions for reactor vessel void fraction response at the beginning of time events

Time event	Times t_M/t_P (s)	$D_{\dot{V}_g} = \frac{\Omega^*_{\dot{V}_g,M}}{\Omega^*_{\dot{V}_g,P}}$	$D_{\dot{Q}_{2\phi}} = \frac{\Omega^*_{\dot{Q}_{2\phi},M}}{\Omega^*_{\dot{Q}_{2\phi},P}}$	Dominant phenomena
2,3,4	*31/31*	*0.31*	**1.01**	Period I—initial blowdown before ADS opening. Two phase change (flashing and condensation) is dominant. $\Omega^*_{\dot{Q}_{2\phi}}$ oscillates between $-0.95<\Omega^*_{\dot{Q}_{2\phi}}<0.95$ in both; *M* and *P*. $\Omega^*_{\dot{V}_g}$ is small because liquid phase flows through the break. The dominant phenomenon is well scaled.
5	*32/42*	*0.21*	**1.19**	
6	*113/147*	***0.37***	**1.03**	
7	***184***/*176*	*−93.22*	*−2.17*	Period II—water flashing after ADS opening and volumetric flow out of reactor vessel to containment vessel. The vapor volumetric flow rate outlet $\Omega^*_{\dot{V}_g} \cong -0.5$ is compensated by flashing and boiling steam generation $\Omega^*_{\dot{Q}_{2\phi}} \sim 0.5$.
8	*182/178*	*0*	**1.19**	
9	***133***/*188*	*0*	*−1.02*	
10	***202***/*189*	**0.77**	*0.13*	
11	***183***/*195*	*0.02*	*26.69*	This is the most intensive portion of the transient based on the heat fluxes and volumetric flow rates. Both phenomena are equally important. Only volumetric flow rates are well scaled at some time events. Two-phase change heating and cooling is not formally well scaled based on the values at the event times due to the oscillatory behavior. However, the trends over time are similar as for volumetric flow rates, but with opposite signs.
12	***249***/*285*	**0.95**	*3.1*	
13	***221***/*395*	**0.67**	*−5.92*	
14	*481/620*	**0.93**	*−0.37*	
15	*2150/1612*	**0.99**	**0.99**	
16	***2260***/*1730*	**1.14**	*4.15*	
17	***2230***/*1830*	***2.25***	**0.52**	Period III—long term cooling. This period is not well scaled. The steam outflow from reactor vessel to containment vessel is present in both, *M* and *P*. However, the behavior is distorted. $\Omega^*_{\dot{V}_g}$ is small, $\Omega^*_{\dot{V}_g} \sim 0$, but negative $\Omega^*_{\dot{V}_g} < 0$, in *M*, while $\Omega^*_{\dot{V}_g} \cong -0.4$ in *P*.
18	*2270/3190*	*0.01*	*−6.82*	
19	***31,569***/*20,860*	*0.05*	*−0.82*	
20	*30,790/20,873*	*0.03*	*−5.51*	
21	***40,000***/*22,300*	*0*	*−0.40*	
22	***28,815***/*49,116*	*0*	*3.34*	Two phase change heating and cooling oscillates between $-0.4<\Omega^*_{\dot{Q}_{2\phi}}<0.4$ in *M* (dominance of the boiling in core and condensation in steam generator are switching in time), while condensation in *P*, $\Omega^*_{\dot{Q}_{2\phi}} \cong -0.1$, prevails. This period has low heat fluxes and volumetric flow rates.

Note: **well scaled**, ***distortion first class***, *distortion second class*, *opposite behavior*.

oscillatory behavior. However, the trends over time are similar as for volumetric flow rates, but with opposite signs.

During long-term cooling (III period), the strong oscillatory behavior is present in both, the prototype and model until 30,000 s (see lower Fig. 17). After 30,000 s, the prototype $\Omega^*_{2\phi,P} \approx -0.1$, while the model oscillates around $\Omega^*_{2\phi,M} \approx 0$ with an amplitude of ± 0.35. It can be concluded that this period is not well scaled. However, this period has low heat fluxes and volumetric flow rates and calculated distortions might be affected by small values of normalized fractional change (effect metrics), or code numerical errors.

Based on all this, an evaluation of the distortions at the beginning of time events (as in Table 7) might result, in some cases, in misleading conclusions. Instead, the qualitative comparisons of time histories provide better insight if some test facility design improvements are possible and if the mass, area, and distribution of internal heat sources, or sinks in the model and adjustments of steam generator (acting as a condenser), and emergency heat removal heat exchanger tube thickness and sizes might produce continuous condensation during the long-term cooling (after 30,000 s) as in the prototype. For example, some other facility with thinner walls, because there is no need to maintain pressure barrier, might be considered as more adequate for the long term cooling period of the transient.

All presented emphasizes importance to understand the time histories of individual processes in both: prototype and model, and evaluate if the model is well scaled based on several criteria and several time periods with different durations. The time periods for the distortion evaluations might need to be shorter at the beginning of the transient because the processes are then usually more intensive and very often there is one or two which are dominant. Also, the time intervals between control system actions (which are reconfiguring the system components connections) are shorter at the beginning of transients. However, only certain actions of the control system produce noticeable changes in the fractional changes of present processes. Based on this, several consecutive time sequences (which were necessary for the correctness of the analysis—to be able to capture reconfigurations of the components connections) might be joined to evaluate distortions. This is even more acceptable for longer periods at the final stages of transients (like long term cooling) when the present processes

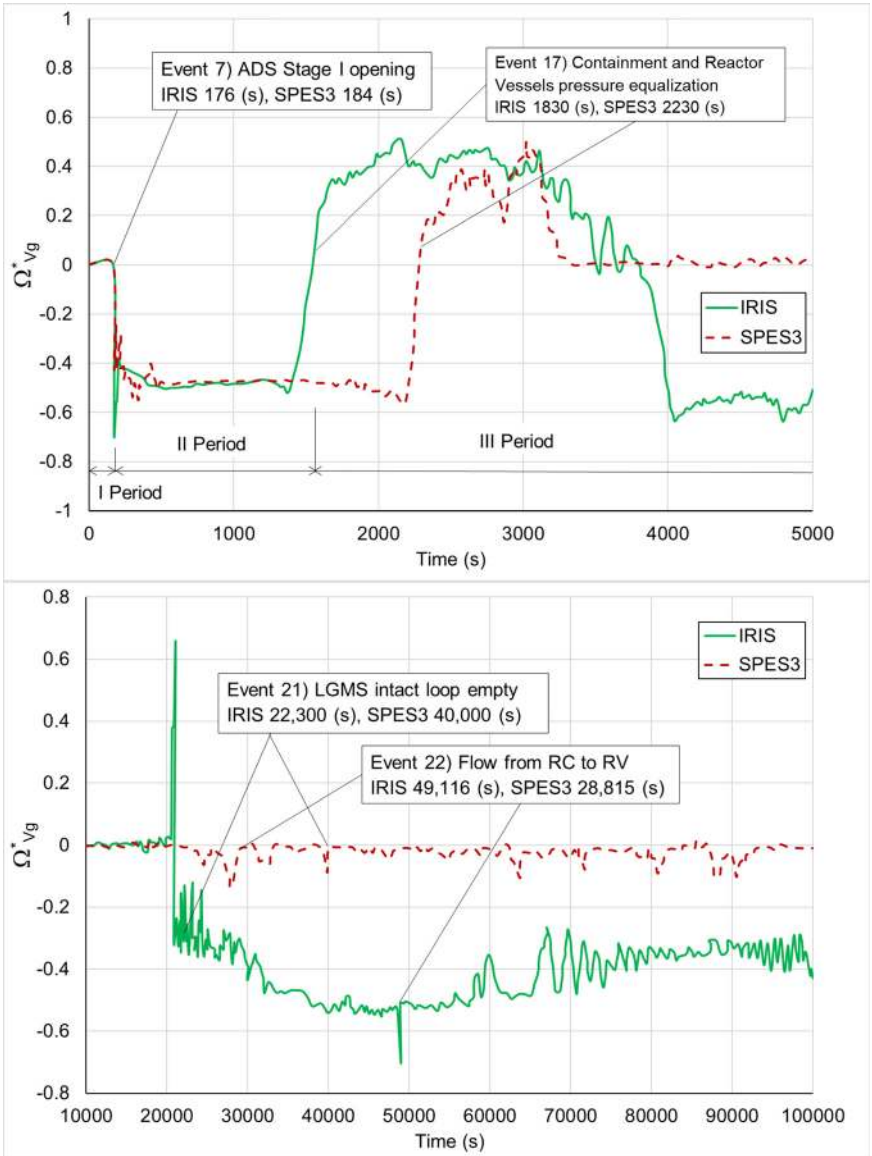

Fig. 16 Normalized fractional changes (effect metrics) for IRIS and SPES3 vapor volumetric flow rate $\Omega^*_{V_g}$ for reactor vessel collapsed water level response as functions of time

are not usually intensive and several of them of similar importance are competing with each other. As discussed earlier, the comparison of the time histories of individual processes in the prototype and the model will provide understanding of the reasons for the present similarities and differences in the prototype and model responses and prevent claims that the model is well scaled even if responses of the individual processes in the prototype and model are acting in opposite directions (for example, $\Omega_{j,P} > 0$ and $\Omega_{j,M} < 0$, or vice versa).

Bottom–Up Process Scaling Analysis. Once when the important processes are established during top–down system scaling analysis, the detailed scaling analysis of important processes might be performed during the bottom–up stage. Due to the complexity of the system and its reconfigurations during multiple time sequences, presenting all details of the bottom–up process scaling analysis is out of the scope of this paper. This part of scaling analysis might be divided in segments and some of them might have higher priority.

The detailed analysis for the most important time sequences and analysis for certain system components (after extracting initial and boundary conditions) where the important process is present, or where the origin of the distortion is suspected, might be performed first.

To gain better understanding of the important process, the terms in Eqs. (4) and (19) might be presented as the summation of multiple terms representing separate subprocesses contributing to the overall process. For example, the two-phase heat transfer term $\dot{Q}_{2\phi}$ might be subdivided in the terms representing two-phase heat transfer due to the flashing, boiling, or condensation so that contributions of each subprocess can be evaluated and conditions for applied heat transfer correlations in the evaluation models checked.

In some cases, due to the lack of the adequate correlations (or existing ones but not valid for necessary range of fluid and flow conditions), the designs of the prototype and model were changed by applying the redesign of components for which test data and correlations in the appropriate range already existed (see Ref. [10]). Also, for some important processes, the correlations were tested and updated (for example, see Ref. [36]).

In some cases, the applied nodalization in evaluation models was adjusted so that modeling of some important processes and interactions between components (or subvolumes inside them—see Fig. 12) might be improved (see Ref. [10]).

By doing so, the designs of the prototype and model, the evaluation models and scaling analysis were iteratively improved (see back bold arrows in Fig. 3). The details of step-by-step development and improvements of the test facility are presented in Ref. [10]. Figures 18 and 19 present comparisons between the prototype and model containment pressure and reactor vessel liquid water mass time histories, respectively, for the final design of the test facility (model) presented in Ref. [10]. The role of scaling analysis in the process of improving the test facility design is partially presented by Ferri and Bianchi [23]. It could be concluded that the final test facility design responses are much closer to the prototype time histories than for the initial design (also presented in Ref. [10]).

Except at the beginning of the transient when the model containment pressure peak is lower and delayed, the rest of the time the model containment pressure is higher than in the prototype and thus on the conservative side (see Fig. 18). The model reactor vessel void fraction and mass of liquid water response are also on conservative side (void fraction is higher and mass of liquid water is smaller than in the prototype) during the majority of the transient except between 20,000 and 30,000 s (see Fig. 19).

However, in spite of the prototype and model similar responses, based on the presented discussions about existing distortions and combined effects of the two processes producing similar responses, but having individually different behavior, there are still possibilities for the test facility improvements, or for planning to test some portions of the transient separately, or even in other test facilities. One example is long-term cooling period at the end of the transient when two low intensity processes are competing with each other.

The bottom–up process scaling analysis provides also an opportunity for the test designers and planners to indicate necessary types and distribution of the instrumentation and specify the frequency of measurements and way of processing of the collected data so that dimensionless numbers used in the scaling analysis (fractional rates Ω in FSA case) can be quantified (see Refs. [24] and [25] for some examples).

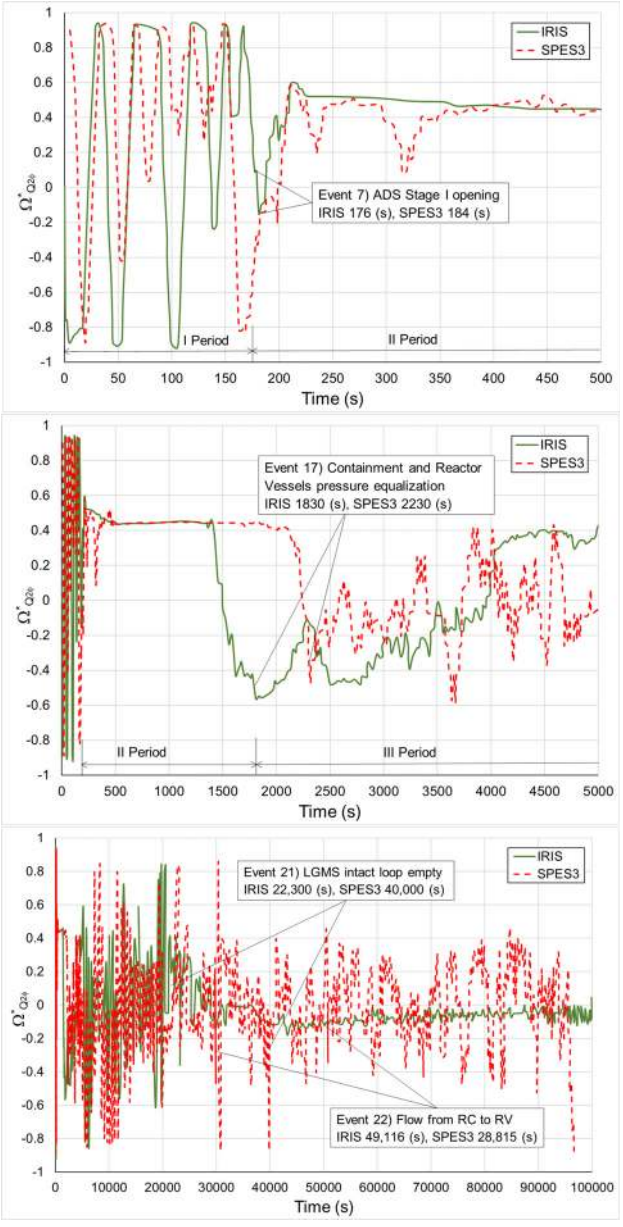

Fig. 17 Normalized fractional changes (effect metrics) for IRIS and SPES3 two phase change heating/cooling $\Omega^*_{Q_{2\phi}}$ for reactor vessel collapsed water level response as functions of time

Conclusions

Details of FSA application for a system with various connections between multiple components during complex transient accident scenario divided in several time sequences are presented.

The system space decomposition in components and time decomposition of the postulated transient accident scenario into time sequences needs to be performed first so that all existing processes can be evaluated and compared. The beginning of the new time sequence might be defined by initiation of the pipe break, actions of the control system (like valves opening, or closing), activating, or de-activating some components (like pumps, core power, heat exchangers), and occurrence, or disappearance of some processes in some components.

Options for deriving and quantifying nondimensional groups for the present processes, like fractional changes (effect metrics), and evaluation of distortions between the prototype and model responses acceptability were presented and discussed. It was concluded that multiple ways of evaluating distortions are necessary.

Distortions based on the instant normalized fractional changes (effect metrics) existing at the beginning of the time sequences ($(D_j)_0 = (\Omega^*_{j,M})_0/(\Omega^*_{j,P})_0$) might in many cases produce conclusions that the model is not well designed and scaled although there is a good qualitative agreement of the prototype and model responses over longer periods. The reason for this is that the beginning of the time sequence is the most challenging moment for the system response because at that moment, one dominant process or combination of several different processes might be initiated. The slight mismatch in timing (in fact delays) of the prototype and model time sequence start, or different order of the prototype and model consecutive time sequences (due to the inability of the model to reproduce exactly the same order) might produce formally unacceptable instant distortions, while the qualitative agreement of the responses in time exists.

One alternative, used in this paper (in combination with quantifying the distortions at beginning of the time sequences, $(D_j)_0$), is to compare the prototype and model normalized fractional changes time histories for each process qualitatively and establish periods when the prototype and model responses are in agreement, or not. This provides an opportunity to indicate potential improvements in the model design, and redefine time sequences, or time periods for distortions quantifications, to improve scaling analysis and test plans and indicate needed test instrumentation and measuring data postprocessing.

The paper presents also a portion of an iterative application of the evaluation models to support the first three elements of EMDAP procedure (see Fig. 3). During that process, the applied evaluation models were improved as well by adjusting nodalizations, improving models for some system components and connections among them, and improving, or replacing heat transfer correlations. The final goal of EMDAP procedure is to make an

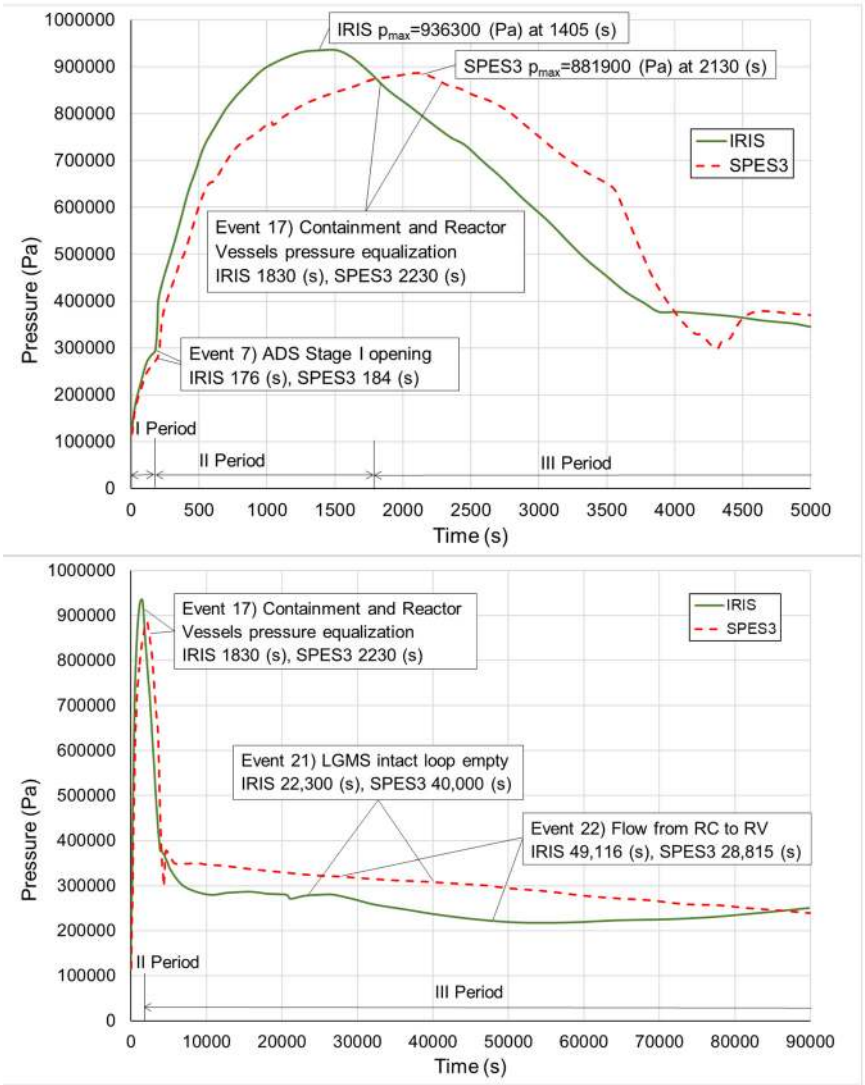

Fig. 18 Comparison of SPES3 and IRIS containment pressure during DVI-SBLOCA transient

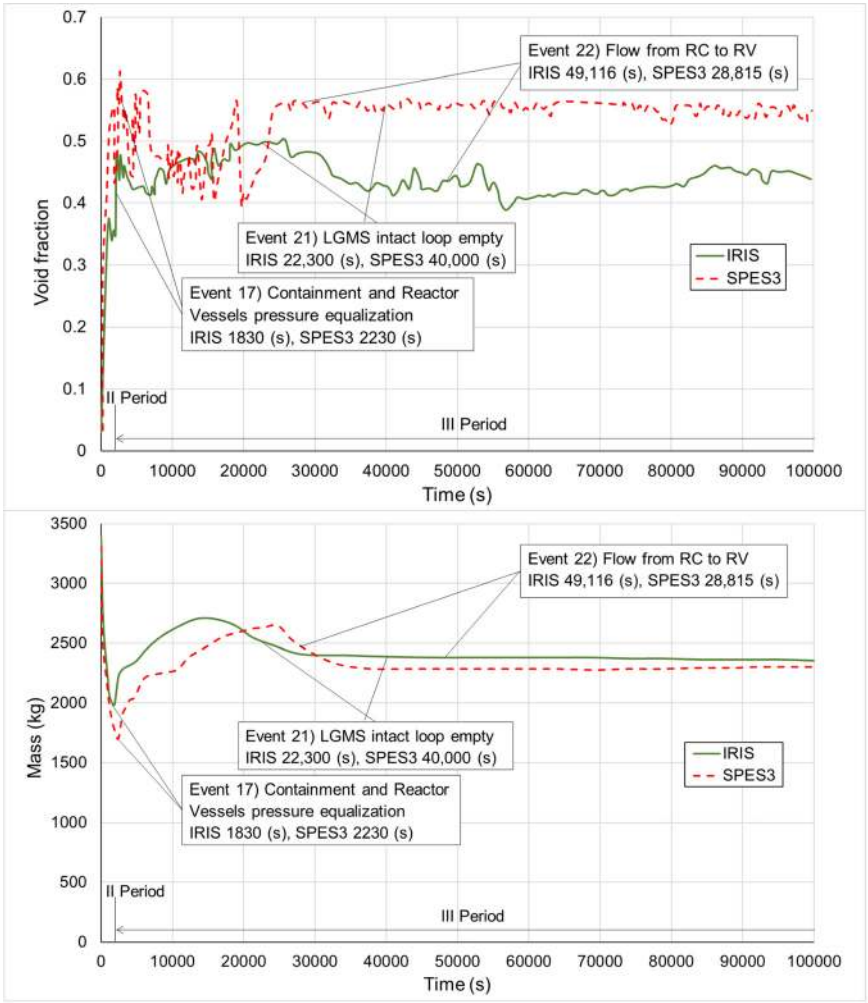

Fig. 19 Comparison of SPES3 and IRIS reactor vessel void fraction and mass during DVI-SBLOCA transient

adequacy decision for the evaluation models intended to be used for simulation of the postulated transient accident scenarios of the real plant (prototype).

An early implementation of the evaluation model to support scaling analysis (EMDAP, element 2, step 6, in Fig. 3) and PIRT quantification (EMDAP, element 1, step 4, in Fig. 3) improves chances for the positive decision of its adequacy by iteratively improving it.

Also, due to the complexities of the system (number of components and possible interactions among them) and postulated transient accident scenarios (number of time sequences, number of present processes, and their time histories), it would be difficult to perform presented scaling analysis without an evaluation method support and most likely some important interactions between components and combined effects of different process on the prototype and model figures of merits response time histories would not been captured.

The first PIRT attempt needs to be performed without an evaluation model help and needs to provide guidance for the first setup of the evaluation model, because if the process is not identified in PIRT, it will most likely not be modeled later on. However, it seems that for scaling analysis of the complex systems and transients, the opposite approach might need to be used. The evaluation model might need to be used iteratively several times and could be some preliminary tests need to be performed as well (to gather data about all possible interactions between present processes) to be able to finally quantify all nondimensional groups and distortions without an evaluation model help.

The FSA application that was presented supports both a satisfactory process for designing an experiment and judging the adequacy of the applied software.

Nomenclature

List of Symbols

c_p = isobaric specific heat, J/kg K
c_v = isochoric specific heat, J/kg K
D = distortion, ratio of model and prototype fractional changes; (Ω^*_M/Ω^*_P)
h = enthalpy, J/kg
K_s = compliance—isentropic compressibility, m^2/N
$\dot{m}$ = mass flow rate, kg/s
p = pressure, Pa
P = power, W
$\dot{Q}$ = heat transfer rate, W
t = time, s
T = temperature, K
V = volume, m^3
v_{fg} = difference of specific volumes, m^3/kg
$\dot{V}$ = volumetric flow rate, m^3/s

Greek Symbols

α = void fraction
β = thermal expansion coefficient, 1/K
γ = ratio of specific heats; (c_p/c_v)

δ = small change
κ = isothermal compressibility, m^2/N
κ_s = isentropic compressibility, m^2/N
ρ = density, m^3/kg
Σ = summation
Φ = agent of change
ψ = state variable
Ψ_α = multiplier in Eqs. (12) and (13), see Eq. (14)
ω = fractional rate of change, 1/s
Ω = fractional change (effect metrics)

List of Subscripts and Superscripts

ADS = automatic depressurization system
bk = break
e = effective fractional rate of change
f = fluid (liquid)
fg = fluid (liquid) and gas
g = gas, vapor
in = into the control volume
int = interface
j = index of summation
k = index of phase
l = liquid
M = model
max = maximum
min = minimum
N_2 = nitrogen
net = net gain or loss
out = out the control volume
P = prototype
PP = pump power
sat = saturation
sys = system
t = time
T = temperature
v = vapor
Δ = difference
ρ = density
0 = initial conditions at start of the time sequence, or reference value
$1\phi l$ = single phase liquid
$1\phi v$ = single phase vapor
2ϕ = two phase

Symbols

$*$ = dimensionless, normalized
$\cdot$ = rate
$'$ = along the saturation line

Acronyms

ADS = automatic depressurization system
AOV = air operating valve
BYP = by-pass
CA = reactor vessel cavity
CORE = core
DC = down comer
DVI = direct vessel injection
DVI_BR = direct vessel injection line in BRoken loop
DVI_IN = direct vessel injection line in INtact loop
DW = dry well
EBS_BR = Emergency Boration System in BRoken loop
EBS_IN = Emergency Boration System in INtact loop
EHRS = emergency heat removal system
EMDAP = Evaluation Model Development and Assessment Process
ENEA = Italian National Agency for New Technologies, Energy, and Sustainable Economic Development
FER = Faculty of Electrical Engineering and Computing
FSA = fractional scaling analysis
GOTHIC = Generation of Thermal-Hydraulic Information for Containment
H2TS = hierarchical, two-tiered scaling analysis
IET = integral effects test
LGMS = long term gravity makeup system tank
LP = lower plenum
IRIS = International Reactor Innovative and Secure
NRC = Nuclear Regulatory Commission
PIPE = pipe connection of pressure suppression tank and long term gravity makeup system tank
PIRT = phenomena identification and ranking table
PZR = pressurizer
PSP = pump suction plenum
PSS = pressure suppression system tank
PWR = Pressurized Water Reactor
QT = quench tank, tank for automatic depressurization system lines discharge
RCP = reactor coolant pumps
RIS = riser
RELAP = Reactor Excursion and Leak Analysis Program
SCRAM = Safety Control Rods Activation Mechanism
SBLOCA = small break loss of coolant accident
SG = steam generator
SET = separate effects test
SIET = Societa Informazioni Esperienze Termoidrauliche, Piacenza, Italy
SPES3 = Simulatore Pressurizzato per Esperienze di Sicurezza 3 (Pressurized Simulator for Safety Tests)
VENT = pipe connection of dry well and pressure suppression system tank

References

[1] Carelli, M. D., Conway, L. E., Oriani, L., Petrovic, B., Lombardi, C. V., Ricotti, M. E., Barroso, A. C. O., Collado, J. M., Cinotti, L., Todreas, N. E., Grgic, D., Moraes, M. M., Boroughs, R. D., Ninokata, H., Ingersoll, D. T., and Oriolo, F., 2004, "The Design and Safety Features of the IRIS Reactor," Nucl. Eng. Des., **230**(1–3), pp. 151–167.
[2] Grgić, D., Bajs, T., Oriani, L., and Conway, L. E., 2003, "Coupled RELAP/GOTHIC Model for IRIS Rector SBLOCA Analysis," International Congress on Advances in Nuclear Power Plants (ICAPP 2003), Cordoba, Spain, May 4–7, Paper No. 3301.
[3] Grgić, D., Čavlina, N., Bajs, T., Oriani, L., and Conway, L. E., 2004, "Coupled RELAP/GOTHIC Code for IRIS SBLOCA Analysis," International Conference on Nuclear Option in Countries With Small and Medium Electricity Grids, Dubrovnik, Croatia, May 16–20, p. 15.
[4] Papini, D., Cammi, A., Ricotti, M., and Grgić, D., 2009, "Analysis of Different Containment Models for IRIS Small Break LOCA, Using GOTHIC and RELAP5 Codes," International Conference on Nuclear Energy for New Europe, Bled, Slovenia, Sept. 14–17, pp. 714.1–714.10.
[5] Papini, D., Grgić, D., Cammi, A., and Ricotti, M., 2011, "Analysis of Different Containment Models for IRIS Small Break LOCA, Using GOTHIC and RELAP5 Codes," Nucl. Eng. Des., **241**(4), pp. 1152–1164.
[6] U.S. NRC, 2005, "Regulatory Guide 1.203, 'Transient and Accident Analysis Methods,'" U.S. NRC, Washington, DC, accessed Jan. 18, 2019, https://www.nrc.gov/docs/ML0535/ML053500170.pdf
[7] Larson, T. K., Moody, F. J., Wilson, G. E., Brown, W. L., Frepoli, C., Hartz, J., Woods, B. G., and Oriani, L., 2007, "Iris Small Break LOCA Phenomena Identification and Ranking Table (PIRT)," Nucl. Eng. Des., **237**(6), pp. 618–626.
[8] Carelli, M., Conway, L., Dzodzo, M., Maioli, A., Oriani, L., Storrick, G., Petrovic, B., Achilli, A., Cattadori, G., Congiu, C., Ferri, R., Ricotti, M., Papini, D., Bianchi, F., Meloni, P., Monti, S., Berra, F., Grgic, D., Yoder, G., and Alemberti, A., 2009, "The SPES3 Experimental Facility Design for the IRIS Reactor Simulation," Sci. Technol. Nucl. Install., **2009**, p. 579430.
[9] Bianchi, F., and Ferri, R., 2010, "SPES3-IRIS Facility RELAP5 Sensitivity Analyses on the Containment System for Design Review," ENEA Ricerca Sistema Elettrico, Piacenza, Italy, Report No. NNFISS-LP2-017.
[10] Achili, A., Congiu, C., Ferri, R., Bianchi, F., Meloni, P., Grgic, D., and Dzodzo, M., 2012, "SPES3 Facility RELAP5 Sensitivity Analyses on the Containment System for Design Review," Sci. Technol. Nucl. Install., **2012**, p. 173637.
[11] Ransom, V. H., Wang, W., and Ishii, M., 1998, "Use of an Ideal Scaled Model for Scaling Evaluation," Nucl. Eng. Des., **186**(1–2), pp. 135–147.
[12] D'Auria, F., and Galassi, G. M., 2010, "Scaling in Nuclear Reactor System Thermal Hydraulics," Nucl. Eng. Des., **240**(10), pp. 3267–3293.
[13] Zuber, N., Wulff, W., Rohatgi, U. S., and Caton, I., 2005, "Application of Fractional Scaling Analysis (FSA) to Loss of Coolant Accidents (LOCA)—Part 1: Methodology Development," 11th International Topical Meeting on Nuclear Reactor Thermal-Hydraulics (NURETH-11), Avignon, France, Oct. 2–6, Paper No. 153.

[14] Wulff, W., Zuber, N., Rohatgi, U. S., and Catton, I., 2005, "Application of Fractional Scaling Analysis (FSA) to Loss of Coolant Accidents (LOCA)—Part 2: System Level Scaling for System Depressurization," 11th Topical Meeting on Nuclear Reactor Thermal-Hydraulics (NURETH-11), Avignon, France, Oct. 2–6, Paper No. 111.
[15] Wulff, W., and Rohatgi, U. S., 1998, "System Scaling for the Westinghouse AP600 Pressurized Water: Reactor and Related Test Facilities," Analysis and Results, U.S. Nuclear Regulatory Commission, Washington, DC, Report No. NUREG/CR-5541.
[16] Catton, I., Wulff, W., Zuber, N., and Rohatgi, U. S., 2005, "Application of Fractional Scaling Analysis (FSA) to Loss of Coolant Accidents (LOCA)—Part 3: Component Level Scaling for Peak Clad Temperature," 11th Topical Meeting on Nuclear Reactor Thermal-Hydraulics (NURETH-11), Avignon, France, Oct. 2–6, Paper No. 055.
[17] Zuber, N., 1991, "A Hierarchical, Two-Tiered Scaling Analysis: Appendix D of An Integrated Structure and Scaling Methodology for Severe Accident Technical Issue Resolution," U. S. Nuclear Regulatory Commission, Washington, DC, Report No. NUREG/CR-5809.
[18] Zuber, N., Wilson, G. E., Ishii, M., Wulff, W., Boyack, B. E., Dukler, A. E., Griffith, P., Healzer, J. M., Henry, R. E., Lehner, J. R., Levy, S., Moody, F. J., Pilch, M., Sehgal, B. R., Spencer, B. W., Theofanous, T. G., and Valente, J., 1998, "An Integrated Structure and Scaling Methodology for Severe Accident Technical Issue Resolution: Development of Methodology," Nucl. Eng. Des., **186**(1–2), pp. 1–21.
[19] Zuber, N., 1999, "A General Method for Scaling and Analyzing Transport Processes," *Applied Optical Measurements*, M. Lehner, and D. Mewes, eds., Springer Verlag, New York, pp. 421–459.
[20] Mesarovic, M. D., Macko, D., and Takahara, Y., 1970, *Theory of Hierarchical Multilevel Systems*, Academic Press, New York, p. 294.
[21] Chow, T. H., ed., 1986, *Time Scale Modeling of Dynamic Networks and Applications to Power Systems*, Springer Verlag, New York.
[22] Kline, S. T., 1986, *Similitude and Approximation Theory*, Springer, New York, p. 229.
[23] Ferri, R., and Bianchi, F., 2010, "Follow-Up of IRIS Design in Support to the Development of the SPES-3 Facility," ENEA Ricerca di Sistema Elettrico, Piacenza, Italy, Report No. NNFISS-LP2-018.
[24] Greco, M., Ferri, R., Achilli, A., Gandolfi, S., Congio, C., Cattadori, G., Bianchi, F., Monti, S., Luce, S., Bertani, C., Mosetto, A., and Dzodzo, M., 2010, "Two-Phase Flow Measurement Studies for the SPES3 Integral Test Facility for IRIS Reactor Simulation," 18th International Conference on Nuclear Engineering (ICONE18-29306), Xi'an, China, May 17–21, pp. 305–316.
[25] Bertani, C., De Salve, M., Malandrone, M., Monni, G., Panella, B., and Mosetto, A., 2010, "SPES-3 Facility Analysis, Reference Data for Postulated Accident Simulation, Criteria for General and Special Instrumentation Selection," ENEA Ricerca di Sistema Elettrico, Torino, Italy, Report No. RdS/2010/68.
[26] Mosetto, A., 2010, "Investigation of the Two-Phase Flow Instrumentation Necessary for the SPES3 Facility," M.Sc. thesis, Politecnico di Torino, Dipartimento di Energetica, Torino, Italy.
[27] Haar, L., Gallagher, J. S., and Kell, G. S., 1984, *NBS/NRC Steam Tables, Thermodynamic and Transport Properties and Computer Programs for Vapor and Liquid States of Water*, Hemisphere Press, New York, p. 320.
[28] Carnevali, S., 2007, "Scaling Studies in Support to the Analysis of IRIS Reactor Pressure Response During LOCAs," M.Sc. thesis, Pisa University, Faculty of Engineering, Pisa, Italy.
[29] Martiello, F., 2008, "Fractional Scaling Analysis of IRIS Reactor and SPES3 Facility for SBLOCA Accident," M.Sc. thesis, Faculty of Engineering, Pisa University, Pisa, Italy.
[30] Lioce, D., 2009, "Application of Fractional Scaling Analysis to IRIS Reactor and SPES3 Facility for SBLOCA Pressure Response," M.Sc. thesis, Faculty of Engineering, Pisa University, Pisa, Italy.
[31] Tortora, G., 2009, "Application of Fractional Scaling Analysis for IRIS and SPES3 Containment Vessels Pressure Responses During DVI-SBLOCA Event," M.Sc. thesis, Faculty of Engineering and Process Industry, Politecnico di Milano, Milano, Italy.
[32] Carnevali, A., 2009, "Application of Fractional Rate of Change Analysis for IRIS-SPES3 Scaling," M.Sc. thesis, Faculty of Engineering, Pisa University, Pisa, Italy.
[33] Dzodzo, M. B., 2009, "EMDAP—Method for Scaling Analysis," 3D S.UN.COP 2009: 10th Seminar, Stockholm, Sweden, Oct. 12–30, pp. 80–82.
[34] Bergamo, S., 2009, "IRIS and SPES3 Reactor Vessel Liquid Level Response Scaling Analysis," M.Sc. thesis, Faculty of Engineering, Pisa University, Pisa, Italy.
[35] Dzodzo, M. B., 2016, "Practical Applications of EMDAP Method for Scaling Analysis," 3D S.UN.COP 2016: 17th Seminar, Seminar, Vienna, Austria, Sept. 12–23, pp. 22–39.
[36] Paini, D., and Ricotti, M. E., 2010, "Follow-Up of SPES3 Experimental Program," ENEA Ricerca di Sistema Elettrico, Piacenza, Italy, Report No. RdS/2010/65.